UCRL-17587

University of California

Ernest O. Lawrence Radiation Laboratory

POLARIZATION CORRELATION OF PHOTONS EMITTED IN AN ATOMIC CASCADE

Carl Alvin Kocher

(Ph. D. Thesis)

May 1967

DISCLAIMER

UCRL-17587

UNIVERSITY OF CALIFORNIA

Lawrence Radiation Laboratory
Berkeley, California

AEC Contract No. W-7405-eng-48

POLARIZATION CORRELATION OF PHOTONS EMITTED IN AN ATOMIC CASCADE

Carl Alvin Kocher

(Ph. D. Thesis)

May 1967

CONTENTS

POLARIZATION CORRELATION OF PHOTONS EMITTED IN AN ATOMIC CASCADE

Carl Alvin Kocher

University of California
Berkeley, California

May, 1967

ABSTRACT

This thesis describes observations of the correlation in linear polarization of two photons emitted successively in an atomic cascade. Calcium atoms in an atomic beam are excited optically ($4^1S_0 \rightarrow 6^1P_1$) by ultraviolet continuum radiation from a high-intensity low-voltage H_2 arc lamp. Photon pairs emitted in the cascade $6^1S_0 \rightarrow 4^1P_1 \rightarrow 4^1S_0$ (5513Å and 4227Å) are detected by conventional photomultipliers fitted with rotatable linear polarizers of the Polaroid type. The coincidence counting rate, recorded by a time-to-height converter and multichannel pulse-height analyzer, is found to be consistent with the theoretical correlation $(\hat{\epsilon}_1 \cdot \hat{\epsilon}_2)^2$, where $\hat{\epsilon}_1$ and $\hat{\epsilon}_2$ denote the observed linear polarizations.

I. INTRODUCTION: AN OUTLINE OF THE EXPERIMENT

One of the most remarkable features of the quantum theory is its prediction of correlations in systems of several particles. A measurement made on one particle can affect the result of a subsequent measurement on another particle of the same system, even though the particles may be non-interacting and separated in space. The experiment described in this thesis is an attempt to observe a photon polarization correlation in a two-stage atomic cascade. An isolated atom, optically excited, returns to the ground state by way of an intermediate state, with the spontaneous emission of two successive photons. Quantum theory predicts that a measurement of the linear polarization of one photon can determine precisely the linear polarization of the other photon.

The plan of the experiment is simple: photon pairs from excited atoms are counted in coincidence, the coincidence rate being recorded as a function of the observed polarizations. If the cascade is chosen so that the photons have wavelengths in the visible region, then the linear polarizers can be of the Polaroid type, and photomultipliers serve as single-photon detectors.

Several major requirements affect the choice of atomic levels for the cascade. First, and most important, the photon energies must be large enough to allow photodetection with high quantum efficiency. In other words, the spectral lines should be near the blue end of the spectrum. Second, the atoms should have zero nuclear spin, for the hyperfine interaction would give rise to a multiplicity of total angular momentum states within each level. If hyperfine structure were present, cascades involving different sets of total angular momentum states

might be observed in the various atoms of the ensemble, and the photon pairs would not necessarily display the same correlation. Finally, the atom must have chemical properties and vapor pressure characteristics which permit the construction of either a resonance bulb or an atomic beam.

After an extensive search through tables of atomic energy levels, the cascade $6^1S_0 \rightarrow 4^1P_1 \rightarrow 4^1S_0$ in calcium (Fig. 1) was selected as the best candidate for the experiment. Calcium vapor reacts with glass and would destroy the transparency of a quartz cell. It is, however, feasible to design an atomic beam oven for calcium. The wavelengths of the cascade photons γ_1 and γ_2 are suitably short: $\lambda_1 = 5513\text{Å}$ and $\lambda_2 = 4227\text{Å}$, respectively. In the naturally occurring mixture of calcium isotopes, virtually all of the atoms (99.87%) have zero nuclear spin [H-2]. The initial atomic state 6^1S_0 is simple, with spherical symmetry, and therefore the method of excitation does not affect the polarizations of the observed photons. Since the 6^1S_0 state cannot be excited directly, the calcium atoms are excited from the ground state to the 6^1P_1 state ($\lambda = 2275\text{Å}$). The excitation radiation is generated by a low-voltage H_2 arc lamp, which emits an intense ultraviolet continuum. A calcium resonance flow-lamp is unsuitable because it would produce a very large undesirable 4227Å background which could not be removed effectively by available filters (Section IV, Part C). Optical interference filters, installed in the excitation lamp (2275Å) and in the detector assemblies (5513Å and 4227Å) are necessary to reduce photomultiplier pickup of stray light from the oven and lamp. A sketch of the basic apparatus is shown

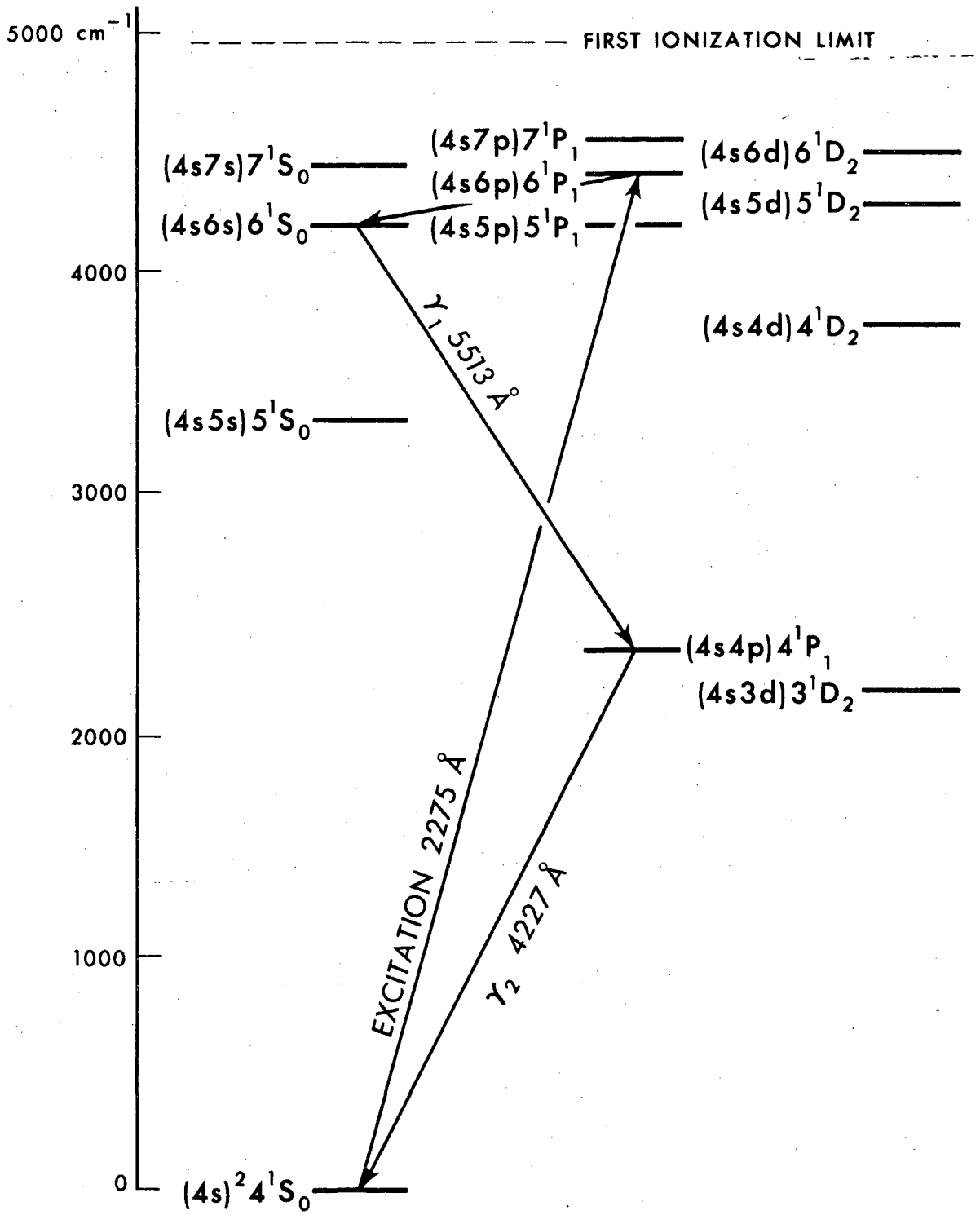

Fig. 1. Level scheme for calcium.

in Fig. 2.

The technique of time analysis permits a direct display of the coincidence rate as a function of delay time. Pulses from the photomultipliers are fed into a time-to-height converter. Its output pulse amplitude, proportional to the time delay between the γ_1 and γ_2 pulses, is analyzed by a multichannel pulse-height analyzer. The exponential decay of the 4^1P_1 state can be observed in this way; its mean life is known to be 4.5×10^{-9} sec [S-4]. Coincidence counts contribute to the time correlation peak in the analyzer display [K-3].

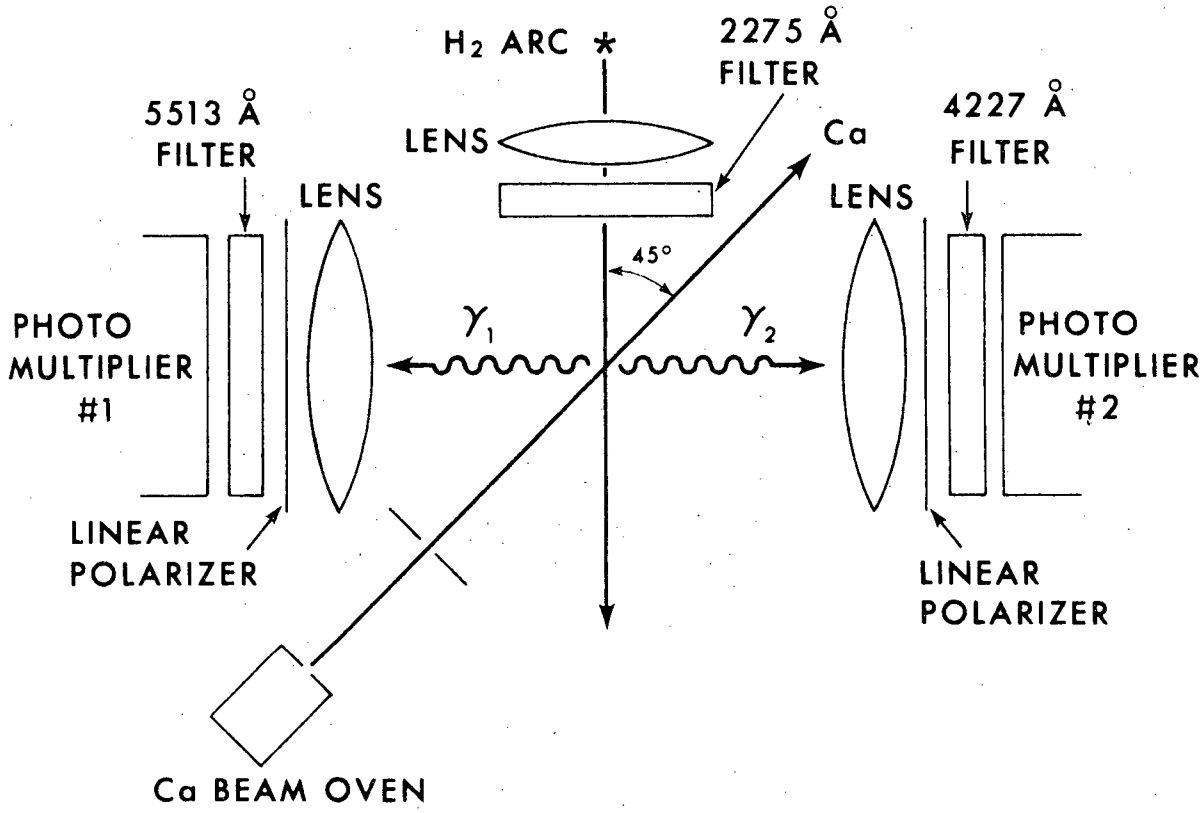

Fig. 2. Schematic diagram of apparatus, top view.

II. THEORY

The theory of polarization correlations is well known. This paper will discuss two approaches to the problem. The first consists of an explicit demonstration that the conservation laws of angular momentum and parity imply a definite correlation in the photon polarizations [F-1, W-2, Y-1]. The second exploits the rotational symmetries of the states which take part in a cascade. Because of its generality, the latter approach is usually taken in the development of the theory of angular correlations of radiations emitted by nuclei [B-6, F-3].

The annihilation of singlet positronium serves as a particularly suitable example of the first method. Linear momentum conservation requires that in the center-of-mass reference frame the two gamma-rays must be emitted in opposite directions, with equal energies. Two polarization states which have the necessary zero total angular momentum are $|++\rangle$ (both photon helicities positive) and $|--\rangle$ (both helicities negative). Since the initial particle-antiparticle pair has odd parity, the correct final state $|\psi\rangle$ is the linear combination of $|++\rangle$ and $|--\rangle$ which has odd parity. $|--\rangle$ is defined to be the state obtained when the parity operator is applied to $|++\rangle$. Consequently, the parity operator transforms $|--\rangle$ into $|++\rangle$. Thus $|\psi\rangle = \frac{1}{\sqrt{2}}[|++\rangle - |--\rangle]$.

To write $|\psi\rangle$ in terms of orthonormal base states $|x\rangle$ and $|y\rangle$ of definite linear polarization, we must define x- and y- axes which are perpendicular to the emission direction. By defining a separate set of axes for each photon, we avoid the inconvenience of a left-handed coordinate system for one of the photons. The z_1- and z_2-axes, in opposite senses,

will be chosen along the propagation directions. The y_1- and y_2-axes will be in the same sense, and the x_1- and x_2-axes will be oppositely directed. For either photon,

$$|+\rangle = \frac{1}{\sqrt{2}}(|x_i\rangle + i|y_i\rangle) \text{ and } |-\rangle = \frac{1}{\sqrt{2}}(|x_i\rangle - i|y_i\rangle).$$

When these states are substituted into the expression for $|\psi\rangle$, the terms having real coefficients subtract away, leaving

$$|\psi\rangle = \frac{i}{\sqrt{2}}[|x_1y_2\rangle + |y_1x_2\rangle].$$

Let φ_1 and φ_2 be the angles between the polarizer axes and the corresponding x-axes. Then the probability amplitude is $\langle\varphi_1\varphi_2|\psi\rangle$ for the observed linear polarization state $|\varphi_1\varphi_2\rangle$. This amplitude is a coherent superposition of the amplitudes $\langle\varphi_1\varphi_2|x_1y_2\rangle$ and $\langle\varphi_1\varphi_2|y_1x_2\rangle$, which interfere to produce the polarization correlation. The coincidence probability is $P = |\langle\varphi_1\varphi_2|\psi\rangle|^2$. This is the probability that both photons are transmitted by the polarizers. Since $|\varphi_i\rangle = \cos\varphi_i|x_i\rangle + \sin\varphi_i|y_i\rangle$, the correlation is given by $P = \frac{1}{2}\sin^2(\varphi_2 + \varphi_1)$ or $P = \frac{1}{2}\sin^2\varphi$, where φ is the angle between the polarizer axes. In particular, the coincidence probabilities for parallel and perpendicular polarizer axes are $P_{\parallel} = 0$ and $P_{\perp} = \frac{1}{2}$.

These arguments may be applied also to the photon pair γ_1, γ_2 emitted in the cascade in calcium. However, by this method it is possible to consider only the special case of antiparallel photon directions. The parities of the initial and final atomic states are even, and therefore the photon state must have even parity:

$$|\psi\rangle = \frac{1}{\sqrt{2}}[|{+}{+}\rangle + |{-}{-}\rangle].$$

The corresponding coincidence probability is $P = \frac{1}{2}\cos^2\varphi$.

The second approach to the polarization correlation calculation will yield this same result. It is a method appropriate for the case of photons emitted by an atom or nucleus, because there will be no restriction on the angle θ between the photon momenta (Fig. 3). As in the positronium example, the coincidence probability is written as the square of a probability amplitude for the transition from the given initial state to the observed final state. The system includes the radiation field as well as the material particles, and the observed final state is characterized by the momenta and polarizations of the emitted photons, as well as by the final state of the atom. If $|i\rangle$, $|m\rangle$, and $|f\rangle$ are the initial, intermediate, and final states, respectively, for the system, and if H' is the interaction Hamiltonian which couples the atom to the radiation field; then the final-state amplitude is the coherent sum

$$a_f \sim \sum_m \langle f|H'|m\rangle\langle m|H'|i\rangle.$$

Constant factors will be dropped, and the time dependence of the amplitudes will be omitted.

In the cascade $6^1S_0 \rightarrow 4^1P_1 \rightarrow 4^1S_0$ in calcium the initial and final atomic states are simple, so that mixed ensembles are not involved. A description of the spontaneous emission of photons requires that the radiation field be quantized. The interaction is

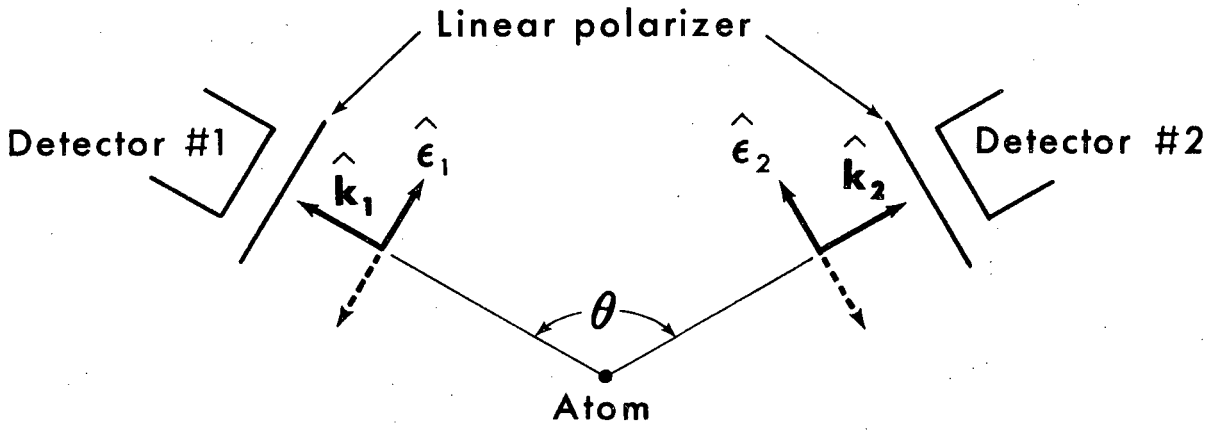

Fig. 3. General γ-γ linear polarization correlation experiment.

$$H' \sim \vec{A}\cdot\vec{p} \sim \frac{1}{\sqrt{\omega}}\,\hat{\epsilon}\cdot\vec{p}\;a^{\dagger}e^{-i\vec{k}\cdot\vec{r}},$$

where $\vec{A}$ is the vector potential, $\vec{p}$ and $\vec{r}$ are the momentum and position of the electron, and where ω and $\vec{k}$ are the energy and momentum of the emitted photon. $\hat{\epsilon}$ is a unit vector in the direction of the photon polarization. The creation operator $a^{\dagger}$ for the observed photon has a radiation-field matrix element equal to unity.

Thus, for electric dipole transitions,

$$a_f \sim \sum_{\substack{m \\ \text{atomic states}}} \langle f|\hat{\epsilon}_2\cdot\vec{r}|m\rangle\langle m|\hat{\epsilon}_1\cdot\vec{r}|i\rangle .$$

In the usual notation $|JM\rangle$ for the atomic states, this expression may be written

$$a_f \sim \sum_{M} \langle 00|\hat{\epsilon}_2\cdot\vec{r}|1M\rangle\langle 1M|\hat{\epsilon}_1\cdot\vec{r}|00\rangle .$$

The operator

$$S \equiv \sum_{M} |1M\rangle\langle 1M|$$

is a scalar with respect to rotations, and the matrix element $\langle 00|\vec{r}\;S\;\vec{r}|00\rangle$ is therefore a multiple of the unit dyadic. Accordingly, $a_f \sim \hat{\epsilon}_1\cdot\hat{\epsilon}_2$ and $P = |a_f|^2 \sim (\hat{\epsilon}_1\cdot\hat{\epsilon}_2)^2$. This result is the probability that the photons γ_1 and γ_2 will be observed with polarizations $\hat{\epsilon}_1$ and $\hat{\epsilon}_2$. It holds for an arbitrary angle θ between the observed photon momenta. If the photon polarizations are not observed, then the coincidence prob-

ability is a sum over the two polarization states for each photon:

$$P \sim \sum_{\hat{\epsilon}_1, \hat{\epsilon}_2} (\hat{\epsilon}_1 \cdot \hat{\epsilon}_2)^2 = 1 + \cos^2 \theta \text{ (angular correlation).}$$

In the experiment of interest, θ is fixed and equal to π. Thus $P = \frac{1}{2} \cos^2 \varphi$, where φ is the angle between the axes of the polarizers, and where the normalization factor $\frac{1}{2}$ is chosen in order that

$$\sum_{\text{polarizations}} P = 1.$$

For an ideal experiment in which there are no accidental coincidences, P would represent the ratio of the coincidence counting rate with the polarizers in place to the rate when they are removed. With the axes of the polarizers parallel and perpendicular, respectively, we expect $P_{\parallel} = \frac{1}{2}$ and $P_{\perp} = 0$.

The effect of an external magnetic field will be considered in Appendix B.

III. THE PROBLEM OF MULTIPLE SCATTERING OF RESONANCE RADIATION

A high coincidence counting rate is desirable but not easily achieved in this type of experiment. The coincidence rate, proportional to the rate at which atoms are excited, increases monotonically with the density of atoms in the atomic beam. Unfortunately, it is necessary to limit the beam density in order to reduce the reabsorption, trapping, and multiple scattering of resonance radiation. These effects result in the loss of photon polarization, discussed in detail by Barrat [B-1]. A semiclassical treatment, to be presented here, is quite adequate for a determination of the maximum beam density which assures negligible multiple scattering of γ_2 photons.

When "white" light passes through an atomic beam, the band of frequencies absorbed in a resonance line will depend on the angle α between the photon momenta and the axis of the beam. If the light is directed along the axis ($\alpha = 0$), the absorption line will show Doppler broadening and a Doppler shift. On the other hand, light directed perpendicular to the beam axis ($\alpha = \frac{\pi}{2}$) will be absorbed only within the natural linewidth. A general value of α will be considered. Let $\mu_N(\omega,\omega')$ denote the absorption coefficient for light of frequency ω passing through an ensemble of stationary atoms whose most probable absorption frequency is ω'. The absorption coefficient is defined to be the probability of absorption per unit macroscopic distance traveled. Similarly, let $\mu(\omega)$ be the absorption coefficient for an ensemble of atoms in motion, such as an atomic beam. The Doppler spread can be described by a distribution $P(\omega')$ such that $P(\omega')d\omega'$ is the probability that an atom has a Doppler-shifted center frequency between ω' and $\omega' + d\omega'$. The absorption

coefficient for the ensemble of moving atoms is

$$\mu(\omega) = \int_0^\infty \mu_N(\omega,\omega')P(\omega')d\omega'.$$

The integral of $\mu(\omega)$ over all frequencies is independent of $P(\omega')$ because

$$\int_0^\infty \mu_N(\omega,\omega')d\omega$$

is independent of ω'. Approximately, $\mu_{D_{max}} \Delta\nu_D \approx \mu_{N_{max}} \Delta\nu_N$. Doppler broadening therefore reduces the absorption coefficient at the center of a resonance line. The natural linewidth for the $4^1P_1 \rightarrow 4^1S_0$ transition in calcium is $\Delta\nu_N \approx 30$ MHz, whereas the maximum Doppler width ($\alpha = 0$) for a calcium beam at 1000° K is $\Delta\nu_D \approx 1000$ MHz. Clearly multiple scattering is far less probable when 4227Å resonance radiation passes along the beam axis than when it is directed perpendicular to this axis.

A similar problem arises when 2275Å continuum radiation is incident on an optically dense calcium beam. After the light has passed only a short distance through the beam, the radiation at the center of the resonance line may have been removed completely. Under these circumstances the total excitation rate decreases slowly as α is increased from 0, and drops very sharply in the immediate vicinity of $\alpha = \frac{\pi}{2}$. For these reasons the experiment is arranged so that neither the excitation light nor the observation axis is directed perpendicular to the atomic beam. The oblique angles are about $\frac{\pi}{4}$ in both cases (Fig. 2).

In an atomic beam the distribution of atomic velocities is

$$P(v) \sim v^3 e^{-\frac{Mv^2}{2kT}},$$

M being the atomic mass and T the source temperature. If the light is

directed at an angle α with respect to the beam axis, then an atom moving with speed v has a most probable absorption frequency ω' given by the Doppler formula

$$\frac{\omega' - \omega_o}{\omega_o} = \frac{v}{c} \cos \alpha,$$

where ω_o is the center frequency for an atom at rest. Thus

$$P(\omega') \sim \begin{cases} (\omega' - \omega_o)^3 \sec^3 \alpha \exp \left[- \frac{Mc^2}{2kT} \left(\frac{\omega' - \omega_o}{\omega_o} \right)^2 \sec^2 \alpha \right] \text{ if } \omega' > \omega_o \\ 0 \text{ if } \omega' < \omega_o. \end{cases}$$

Because $\mu_N(\omega,\omega')$ is much narrower than $P(\omega')$, the shape of $\mu(\omega)$ is determined almost entirely by $P(\omega')$. This approximation is valid except when α is very close to $\frac{\pi}{2}$. If we define $x \equiv \frac{2}{A}(\omega - \omega_o)$, where A is the Einstein spontaneous-emission coefficient for the transition, then

$$\mu(x) = K \sec^3 \alpha \cdot x^3 e^{-\beta x^2} \Theta(x).$$

Here $\Theta(x)$ is the Heaviside unit function and

$$\beta \equiv \frac{Mc^2 A^2 \sec^2 \alpha}{8kT\omega_o^2} = \frac{M\lambda^2 A^2 \sec^2 \alpha}{32\pi^2 kT};$$

λ is the wavelength corresponding to ω_o. The absorption coefficient for the natural line has the Lorentz shape

$$\mu_N(x) = \frac{\mu_o}{1 + x^2}.$$

The peak absorption is

$$\mu_o = \frac{3n\lambda^2}{2\pi} \quad [C\text{-}5, H\text{-}5],$$

where n is the number density of atoms in the beam, and where the factor of 3 is the statistical weight of the P-level. The constant K is determined by the normalization condition

$$\int_{-\infty}^{\infty} \mu(x)dx = \int_{-\infty}^{\infty} \mu_N(x)dx.$$

Thus

$$K \sec^3 \alpha \int_0^{\infty} x^3 e^{-\beta x^2} dx = \mu_o \int_{-\infty}^{\infty} \frac{dx}{1 + x^2},$$

and therefore,

$$K \sec^3 \alpha = 2\pi\beta^2 \mu_o.$$

The peak value attained by $\mu(x)$ is

$$\mu_{max} = 2\pi \left(\frac{2e}{3}\right)^{-3/2} \sqrt{\beta}\ \mu_o = 2.58 \sqrt{\beta}\ \mu_o.$$

μ_{max} is proportional to $\lambda^3 A$, for given values of M, T, n, and α. From Table I, Section IV, the A-coefficients for the relevant resonance transitions are $A_{4227} = 2.2 \times 10^8$ sec^{-1} and $A_{2275} = 3.3 \times 10^7$ sec^{-1}. The ratio of the peak absorption coefficients is

$$\frac{\mu_{max}\ (4227\text{Å})}{\mu_{max}\ (2275\text{Å})} = \left(\frac{4227}{2275}\right)^3 \cdot \frac{2.2 \times 10^8}{3.3 \times 10^7} = 43.$$

The ratio is large, and consequently the limiting value of n is due to multiple scattering of γ_2 photons (4227Å) rather than to loss of excitation (2275Å). The dimensionless parameter β may be treated as a constant, since it varies slowly with the absolute oven temperature T. Numerically, if M = 40 amu, $\lambda = 4.23 \times 10^{-5}$ cm, $A = 2.2 \times 10^8$ sec^{-1}, $\alpha = \frac{\pi}{4}$, and

$T = 1000^{\circ}$ K, we obtain the value $\beta = 2.6 \times 10^{-4}$.

The maximum value of the 4227Å absorption coefficient is therefore $\mu_{max} = 4.2 \times 10^{-2}\ \mu_o$. For an excitation region whose typical dimension is L, multiple scattering will be of minimal consequence if $\mu_{max} \lesssim \frac{1}{L}$. This somewhat arbitrary criterion determines the maximum allowable value of n.

$$n_{max} = \frac{2\pi\mu_o}{3\lambda^2} = \frac{2\pi}{3\lambda^2} \cdot \frac{1}{4.2 \times 10^{-2}\ L}.$$

Taking L = 1 cm for the atomic beam geometry used in the experiment, we find that $n_{max} = 3 \times 10^{10}$ atoms/cm^3. The beam density should not exceed this limit, which is approximately the optimum density.

IV. AN ESTIMATE OF THE COINCIDENCE COUNTING RATE

The calcium atoms are excited from the 4^1S_0 ground state to the 6^1P_1 state (2275Å). The expected rates of emission of the cascade photons γ_1 and γ_2 will depend on various transition rates, in addition to the intensity of the excitation source and the density of the atomic beam. Most important is the branching ratio for the transition $6^1P_1 \rightarrow 6^1S_0$ to the initial state for the cascade. Theoretical transition rate calculations require the evaluation of reduced matrix elements, which are integrals involving radial wave functions. The labor required for numerical integration would be prohibitive. For the present purpose, the transition rates can be computed to sufficient accuracy by means of a Bates-Damgaard calculation [B-2, G-2]. This is a Coulomb approximation, in which the potential is replaced by its asymptotic form.

The Einstein A-coefficients given in Table I were computed by the method of Bates and Damgaard. The term assignments are those of Moore [M-2]. For the 4227Å resonance line there is surprisingly good agreement (within 5%) between the calculated rate and the Hanle-effect measurements reported by Lurio, de Zafra, and Goshen [L-4] and by Smith and Gallagher [S-4]. There is also good agreement (within 20%) with hook-method measurements of relative oscillator strengths for the resonance lines, published by several groups working in the Soviet Union [O-1, O-2, S-3]. Most of these data are restricted to the strongest lines. From Table I we can estimate that as many as 25% (conservatively, at least 10%) of the excited atoms which do not return directly to the ground state will enter the 6^1S_0 state. Since most of

TABLE I. Einstein A-Coefficients for calcium, computed by the Bates-Damgaard approximation

Initial state	Final state	$\lambda(\mathring{A})$	$A(sec^{-1})$
4^1P_1	4^1S_0	4227	2.2×10^8
5^1P_1	4^1S_0	2398	9.5×10^6
	5^1S_0		3.9×10^6
	4^1D_2		1.5×10^6
6^1P_1	4^1S_0	2275	3.3×10^7
	5^1S_0		7.5×10^6
	6^1S_0		3.3×10^6
	4^1D_2		6.0×10^5
	5^1D_2		4.4×10^5
7^1P_1	4^1S_0	2201	7.4×10^6
	5^1S_0		2.8×10^6
	6^1S_0		4.1×10^5
	7^1S_0		1.1×10^6
	4^1D_2		2.5×10^4
	5^1D_2		8.6×10^2
	6^1D_2		1.2×10^3
6^1S_0	4^1P_1	5513	1.6×10^7
	5^1P_1		2.1×10^3
7^1S_0	4^1P_1		7.7×10^6
	5^1P_1		4.2×10^6
	6^1P_1		3.0×10^3

the remaining atoms reach the 4^1P_1 level by other routes, the rate R of γ_2 emission will be about 10 times the rate of γ_1 emission. The single-detector counting rates are $N_1 = 10^{-1}\,\eta_1 R$ and $N_2 = \eta_2 R$, where η_1 and η_2 are the overall efficiencies of the detectors. The expected coincidence rate (with polarizers removed) is $N_c = 10^{-1}\,\eta_1\eta_2 R$. Table I indicates that R should be approximately one fourth of the total excitation rate R_{tot} for the transition $4^1S_0 \rightarrow 6^1P_1$. Thus R can be predicted if we know the density of the atomic beam, the intensity of the excitation light from the H_2 lamp, and the A-coefficient for the $4^1S_0 \rightarrow 6^1P_1$ transition.

When the 2275Å excitation radiation passes through the calcium beam, the transmitted power per unit area and per unit wavelength decreases exponentially with the distance z:

$$I(\lambda) = I_o\, e^{-\mu(\lambda)z}.$$

At the optimum atomic beam density n, the total absorption probability $[1 - e^{-\mu(\lambda)z}]$ at wavelength λ is fairly small for the 4227Å line and even smaller for the 2275Å line. Therefore the exponential can be expanded to yield a simple expression for the power lost in the distance z:

$$P = \sigma z I_o \left|\frac{d\lambda}{dx}\right| \int_{-\infty}^{\infty} \mu(x)dx = \sigma z I_o \frac{\lambda^2 A}{4\pi c} \cdot \pi\mu_o,$$

where σ is the cross-sectional area of the light beam. The volume σz will be set equal to the volume V of the excitation region, which is approximately 0.7 cm^3. If we neglect excitations due to multiple scattering, the total excitation rate at 2275Å is

$$R_{tot} = \frac{P}{\hbar\omega_o} = \frac{3VI_o n\lambda^5 A}{16\pi^2 \hbar c^2} .$$

An intensity measurement taken with a radiation thermopile shows that the ultraviolet intensity at the excitation region is approximately 3×10^2 μwatt/cm^2. This is I_o integrated over the 300Å passband of the interference filter; therefore $I_o \approx 10$ erg/(sec·Å ·cm^2). The geometry of the lamp and the details of the thermopile measurement will be described in Section V, Part C. If $n = 3 \times 10^{10}$/cm^3 and $A = 3.3 \times 10^7$ sec^{-1}, then $R_{tot} \approx 8 \times 10^7$ excitations/sec and $R \approx 10^7$/sec. An additional uncertainty in this value arises from the fact that the 300Å passband of the filter is so broad that P-states other than 6^1P_1 are excited to some extent. The excitation of higher levels, up to the ionization limit at 2028Å, contributes to the useful population of the initial state for the cascade. However, the 5^1P_1 state (2398Å) lies below the 6^1S_0 state, and its excitation contributes only to the number of γ_2 photons not preceded by γ_1 photons. A study of Table I and a knowledge of the transmission spectrum of the filter (Section V, Part D) suggest that these complications should not increase the ratio N_2/N_1 by more than about 40%.

The detector efficiencies η, to be discussed later, will be shown to be approximately 10^{-3}. With these values the predicted coincidence rate is $N_c = 10^{-1}\ \eta_1\eta_2 R \approx 1$ count/sec (polarizers removed). This rough estimate indicated that the polarization correlation experiment could be performed successfully, although long observation times are required. Sources of noise will be considered in a subsequent section.

V. THE EXPERIMENTAL APPARATUS

A. Vacuum System

Figures 4 and 5 show the layout of the source chamber and the adjoining excitation chamber, to which are attached the hydrogen lamp, the detector assemblies, and the vacuum pumps. Brass construction and standard vacuum techniques are employed. Only the two main chambers are evacuated; there are two oil-type diffusion pumps. The source chamber requires a large pump to remove the water vapor and other gases given off when the oven is heated to operating temperature.

A liquid nitrogen trap is included in the top flange for the main chamber. A similar trap attached to the source chamber was found to be unnecessary, as the fresh layer of calcium metal accumulating on the steel bulkhead acts as an efficient getter. The pressure in the source chamber is monitored by a VGIA ion gauge, and is typically 5×10^{-6} Torr during operation of the oven. Cutoff flags for the atomic beam and the excitation light are adjustable through Wilson seals.

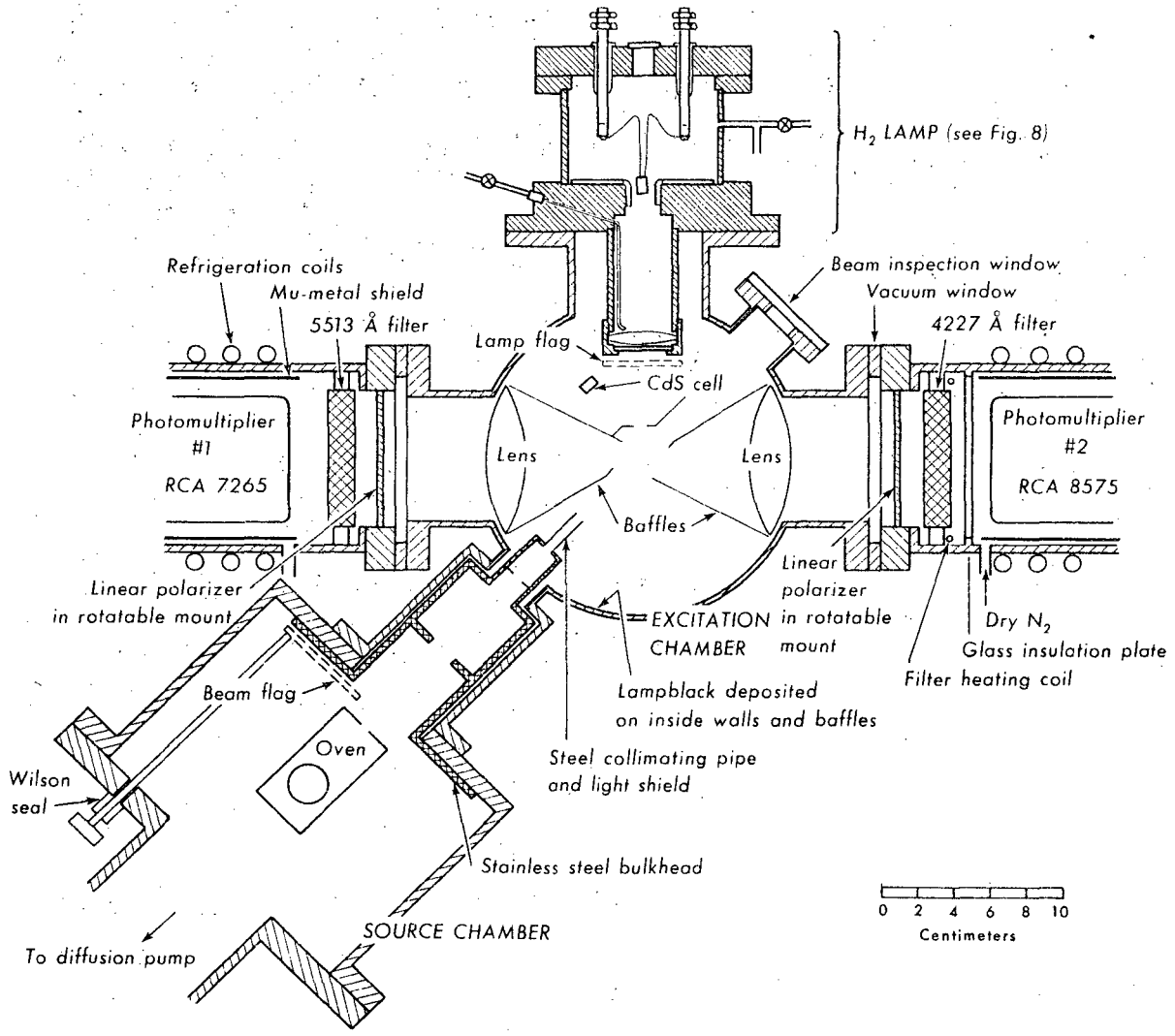

Fig. 4. Cross-section of apparatus, top view.

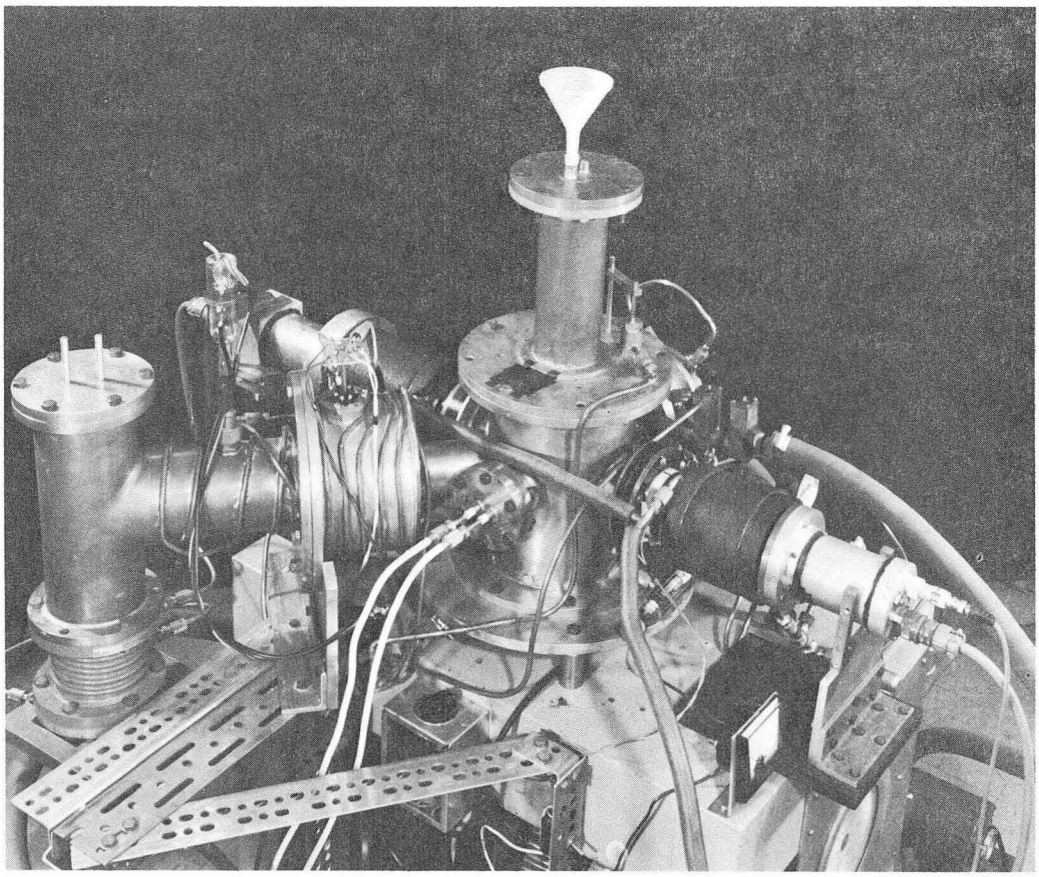

XBB 675-2606

Fig. 5. The apparatus. This photograph shows the source chamber (left center), excitation chamber (center), and photomultiplier assemblies. The excitation lamp is mounted on the far side.

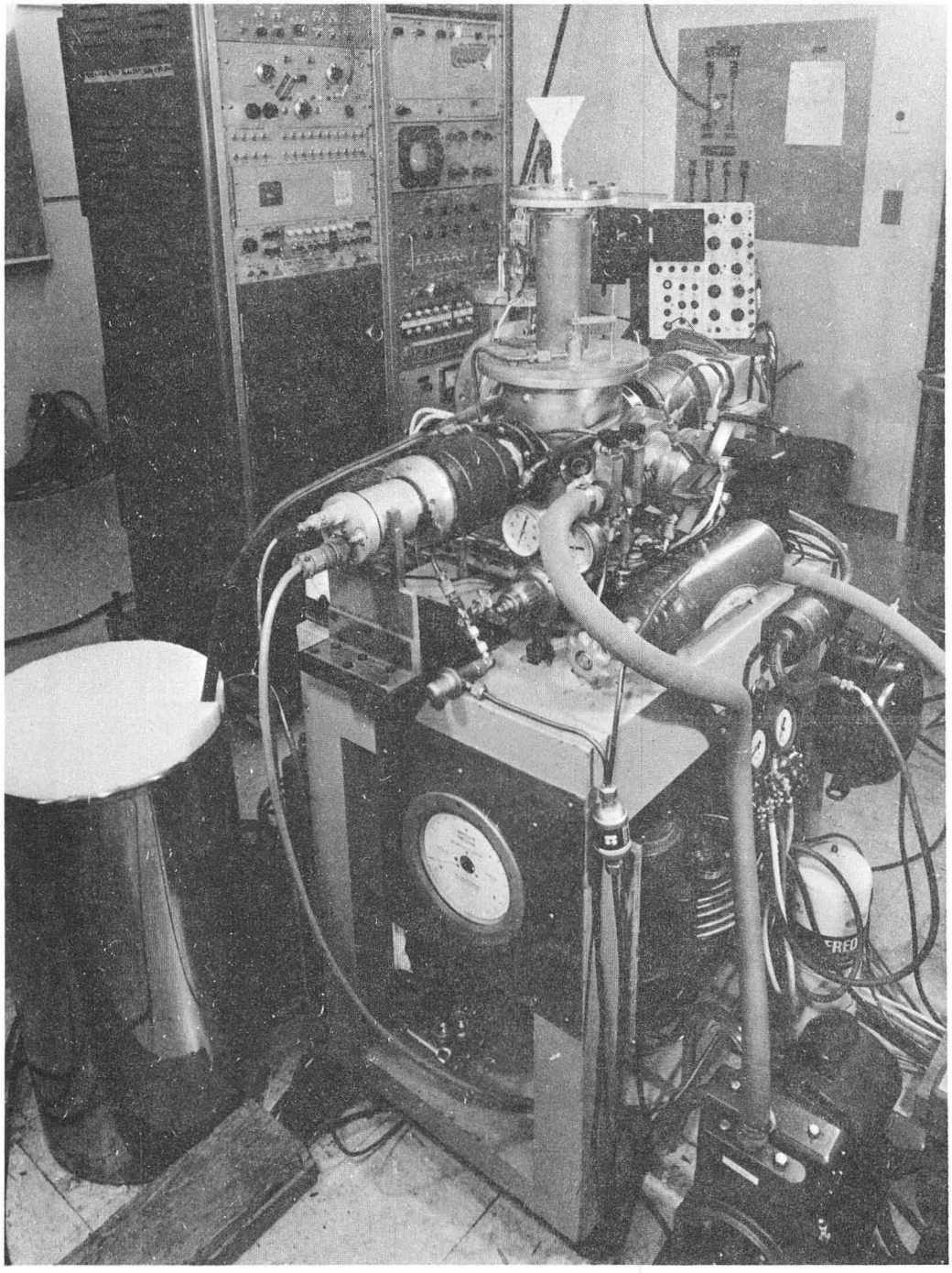

XBB 675-2608

Fig. 6. An overall view of the apparatus. The RCL analyzer is shown in the background.

B. Atomic Beam Oven

The calcium beam oven (Fig. 7) is of large size (6.5 × 3.4 × 4.4 cm) and of conventional design [R-1]. The loading well, located at the rear, is a cylindrical volume 2.0 cm in diameter and 3.0 cm in height, fitted with a tapered plug. A full load consists of about 12 gm of calcium in the form of a solid cylinder, turned down on a lathe to the appropriate size. Eight heating coils surround the well. Extending from the well to the orifice at the front face of the oven is a channel 0.5 cm in diameter, surrounded by sixteen heating coils. The orifice itself is an insert having a circular aperture 0.27 cm in diameter.

Originally the oven was made from cold-rolled steel. However, the inner walls of the well became slightly etched, and calcium leaked out around the edge of the plug. Apparently this difficulty was the result of a chemical reaction between steel and calcium vapor at 1000° K. A satisfactory oven and plug were machined from a block of tantalum.

Thermal isolation for the oven is accomplished by a pin mount and by a horizontal slot which separates the channel region from the bottom surface of the oven. The heating coils are wound from tantalum wire of 0.038-cm diameter and are set in sections of ceramic tubing. Separate variacs control the heaters for the channel and the well. The corresponding temperatures at the front and rear are monitored by chromel-alumel thermocouple junctions inserted into small holes drilled in the top of the oven. The operating temperature at the front is about 25° higher than at the rear, to insure that condensation of calcium vapor does not occur in the channel.

A simple kinetic theory calculation shows that a vapor pressure of

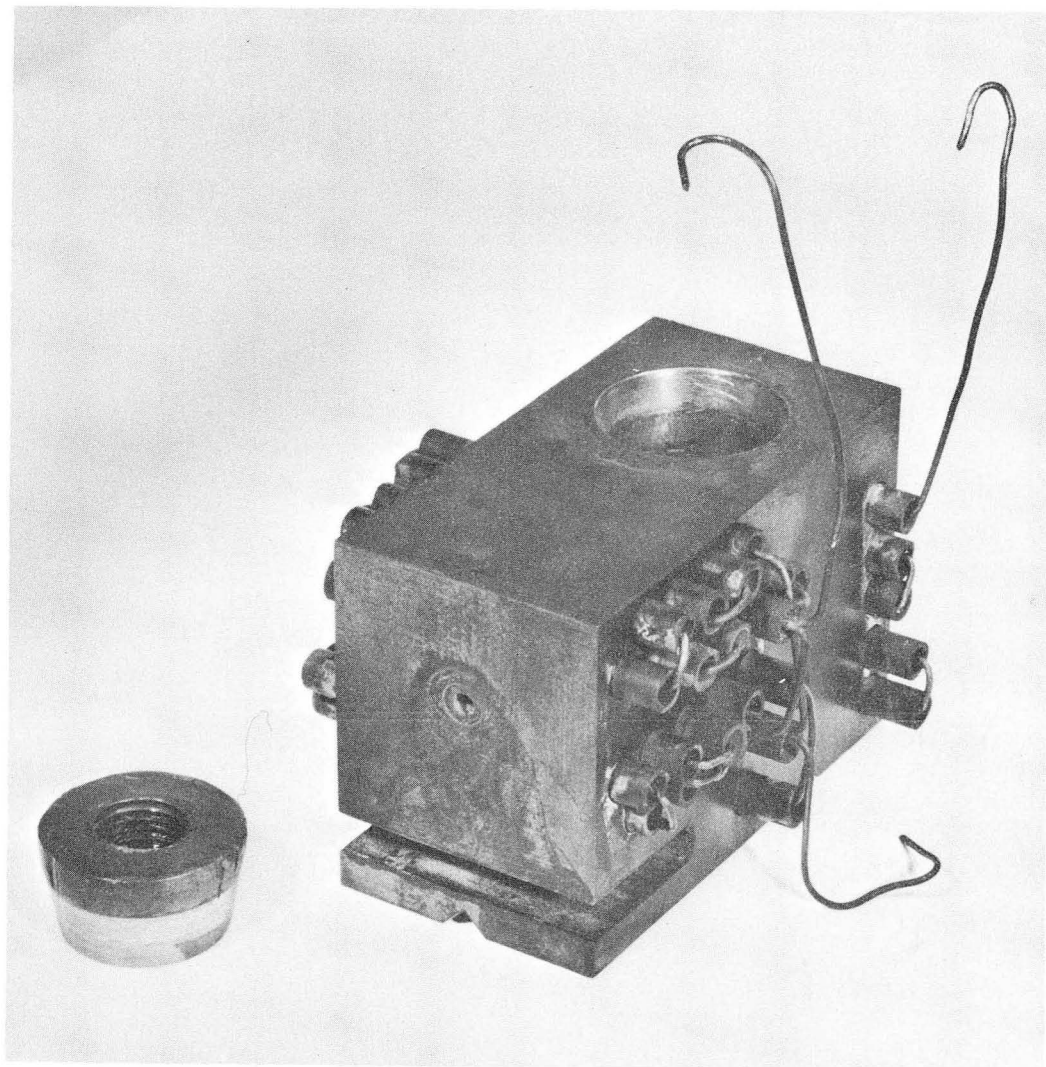

XBB 675-2605

Fig. 7. Atomic beam oven for calcium.

approximately 10^{-1} Torr will provide the optimum beam density $n = 3 \times 10^{10}$ atoms/cm^3 at the excitation region, which is 21 cm from the front of the oven. Calcium attains this vapor pressure at about 1000° K. This operating temperature is reached when the oven heaters dissipate about 550 watts, in rough agreement with the dissipation expected from Stefan's law. Since the vapor pressure varies rapidly with oven temperature, the thermocouple reading does not permit accurate determination of the beam density.

The melting temperature of calcium is 1110° K, somewhat above the normal oven temperature. However, in early tests there was a tendency for the orifice to become obstructed with melted metal. The calcium sample then in use was found to contain aluminum, which melts at 930° K. Substitution of redistilled calcium solved this problem.

When a brass bulkhead was employed in front of the oven, the calcium deposit tended to flake off and fall into the path of the beam. Equally serious, a cloud of calcium vapor was reflected back toward the oven. At high beam densities, the cloud would form an unstable discharge around the oven heaters. The 4227Å resonance radiation emitted by this discharge would scatter into the γ_2 photomultiplier, causing an enormous counting rate of unwanted pulses. A test with a number of metals revealed that calcium would stick well to a bulkhead of stainless steel #304. When a new stainless steel bulkhead and beam-collimating pipe were installed, the discharge did not recur. In addition, the calcium layer adhered so uniformly that the thickness of the deposit could be measured with a micrometer.

The measured thickness of the calcium layer at the first collimating slit permits a reasonably accurate calculation (within 10%) of the quantity of calcium which has passed through in the beam. We can therefore predict the running time t for the desired beam density n:

$$t = \frac{\ell^2 \rho D}{L^2 n} \sqrt{\frac{\pi N_o}{8MkT}} \ ,$$

where ℓ = distance from oven opening to collimating slit = 7 cm

L = distance from oven opening to excitation region = 21 cm

ρ = density of solid Ca = 1.54 gm/cm^3

D = thickness of Ca layer = 0.095 cm after a full oven load has been exhausted

N_o = Avogadro's number

For these values the density $n = 3 \times 10^{10}/cm^3$ will be maintained if $t \approx 30$ hours. There is no simple way to calculate the precise variac settings for this length of run; they are best learned by experience.

C. Excitation Source: A High-Intensity Low-Voltage H_2 Arc of Simplified Design

Special attention must be devoted to the urgent need for obtaining the highest possible excitation rate $4^1S_0 \rightarrow 6^1P_1$ (2275Å) in the atomic beam. In a calcium resonance flow-lamp having a quartz window, this transition would receive about 10^{-4} of the power concentrated in the strongest resonance line (4227Å), $4^1P_1 \rightarrow 4^1S_0$ [G-1]. Even the best available ultraviolet interference filters transmit approximately 0.1% at 4000Å (and no more than 25% at 2275Å). For a flow-lamp with one filter, the intensity ratio I_o (4227Å)/I_o (2275Å) at the excitation region would be about 40. Since μ_{max} (4227Å)/μ_{max} (2275Å) = 43 (Section III), the 4227Å excitation rate in the atomic beam could easily be a disastrous 10^3 times the 2275Å rate. If the 4227Å line were blocked by additional interference filters, there is good reason to doubt that I_o (2275Å) would be sufficient to satisfy the excitation requirement. Excitation by electron bombardment leads to the same difficulty, as again the 4227Å transition would be the most readily excited, because it has by far the largest dipole matrix element.

A high-intensity continuum light source in the ultraviolet offers an attractive solution to the excitation problem. High-voltage mercury and xenon lamps of very high pressure (5 to 20 atmospheres) are commercially available. In quartz envelopes they emit an ultraviolet continuum which might be useful down to 2200Å. In the case of Hg, the spectrum is a quasi-continuum due to pressure broadening of strong spectral lines. In both the Xe and the Hg lamps the spectral density is considerably greater in the visible region than in the vicinity of 2275Å [B-3].

A one-kilowatt Hg lamp having a narrow 0.1-cm diameter capillary (Pek Laboratories type C) was tested as a possible excitation source. The total intensity in the visible region was very high, and could not have been reduced adequately by interference filters. A simple quartz-prism spectrometer was installed between the lamp and the excitation chamber. It was designed to remove the visible light and to pass a 300Å band at 2275Å. Narrow slits were required. Even when the spectrometer was carefully aligned, its output contained excessive visible light, demanding the use of an interference filter at the exit slit. Unfortunately, the intensity at 2275Å was insufficient. After it became clear that this arrangement was unsatisfactory, the search for a more suitable excitation source led to consideration of a molecular hydrogen arc lamp.

The H_2 spectrum displays an ultraviolet continuum which extends from about 4500Å to beyond 1800Å. The spectral profile is smooth in this region, with no discrete lines or other sharp prominences; it has a gradual peak between 2300Å and 2500Å [L-3]. According to the theory of Winans and Stuekelberg [C-2, R-3, W-4], this continuum arises from molecular transitions between the relatively stable $1s\sigma 2s\sigma\,^3\Sigma_g$ excited state and the unstable $1s\sigma 2p\sigma\,^3\Sigma_u$ lower state, which dissociates into unexcited atoms having kinetic energy. Theoretical calculations for these transitions in H_2 and D_2 are in satisfactory agreement with the observed intensity distribution [C-4, J-1]. The large spread in photon energies is due to contributions from a number of vibrational levels belonging to the upper state. For some reason, not well understood, the lamp output may be greater with D_2 gas than with H_2 [S-5].

The highest-intensity H_2 lamp available commercially (the Hanovia lamp) has a large, fragile, glass envelope and requires high voltages (several kilovolts). Low-voltage, high-current H_2 arc lamps have been described which provide between 50 and 100 times the intensity available from commercial H_2 sources [K-4]. A number of articles have been published which furnish construction details for rugged metal-cased low-voltage d.c. arcs, claimed to be reliable and of simple design [A-1, F-2, H-4, R-2]. Except for the lamp described by Rendina [R-2], they are in fact quite intricate and have complicated electrode arrangements.

The Rendina lamp is of brass construction and is easily built. It employs a dispenser cathode of the type pioneered by Hull [H-8]. A d.c. voltage is applied between cathode and anode, and a heating current is passed through the cathode to initiate the discharge by thermionic emission. The cathode consists of a cylindrical molybdenum screen filled with barium aluminate granules. It is protected by a molybdenum shield supported by standoff insulators. The heating current can be turned off during lamp operation, as the cathode is kept hot by positive ion bombardment. The radiation from the discharge passes through an exit hole in the anode, a small aluminum button fitted into the body of the lamp.

The brass lamp body constructed for this experiment (Fig. 8) follows closely the cylindrical design of Rendina. Water cooling is provided for the top and bottom flanges, but not directly for the individual electrodes. A number of electrode configurations similar to Rendina's were tested. In all of the first attempts, the anode became badly pitted, especially

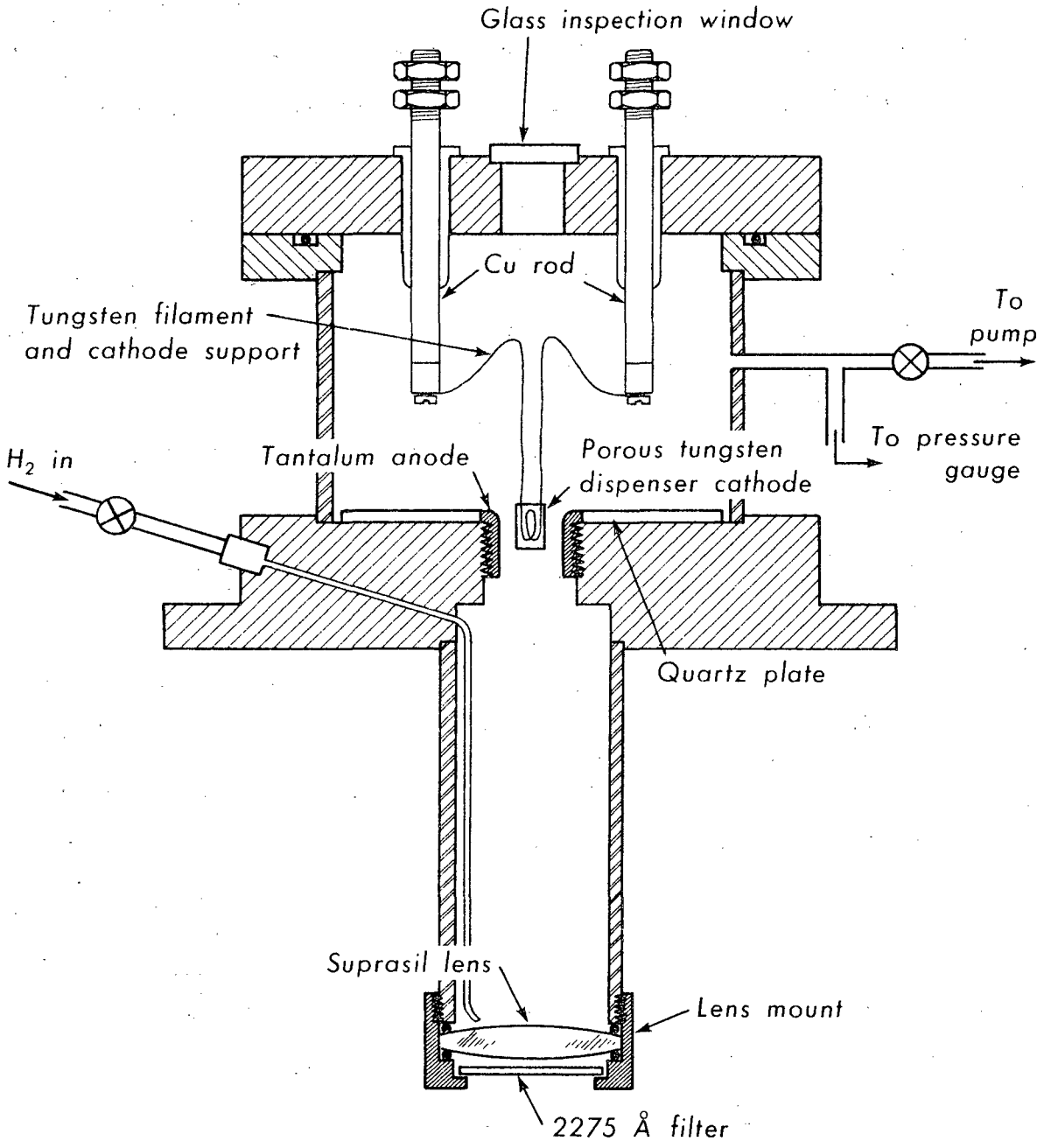

Fig. 8. Molecular hydrogen arc lamp, cross-section.

when the current exceeded 5 amperes. After several hours of operation at 3 amperes, the cathode screen would become brittle and break apart. Experimental cathode coatings with barium and strontium carbonates did not last. Sputtering was so severe that the quartz exit window readily acquired an opaque layer of unidentified material, presumably from the cathode. Under these conditions the discharge was unstable and the ultraviolet intensity was low. These tests were conducted with H_2 pressures of 2 to 5 Torr. It is possible that some of the difficulties just described are attributable to impurities in the H_2, since only a mechanical forepump was used for the initial evacuation of the lamp chamber. However, it seemed worthwhile to experiment further with electrode materials before proceeding to the use of a diffusion pump and the elaborate gas purification systems customarily used with flow lamps [B-14].

The first and most obvious improvement was the replacement of the aluminum anode by a larger hollow cylinder of tantalum, threaded for ease of replacement and for good electrical and thermal contact with the water-cooled brass bottom plate, which is 2.5 cm thick. In the final anode the interior region is 1.4 cm in height and 0.95 cm in diameter. The cathode is mounted not above the anode, as in the Rendina lamp, but almost entirely inside of it. By far the best cathodes, out of many types tested, were porous tungsten dispenser cathodes impregnated with barium aluminate and calcium oxide. They are similar to the cathodes used in high-power vacuum tubes, and were made to order by Spectramat, Inc. The material is known as type 31180, which contains Ba, Ca, and Al, in the ratio 3:1:1. A satisfactory shape is a cylinder,

1.0 cm in length, with inner and outer diameters 0.30 cm and 0.50 cm. The cathode is supported from the feedthroughs by 0.089-cm diameter tungsten wire, as indicated in Figs. 8 and 9. The same tungsten wire serves as the filament, and is heated to incandesence when the lamp is to be started. A Tesla-coil spark is not necessary. After the discharge is sustained, the filament current can be turned off. A spot-weld fastens the cathode to the filament wire, although a tight friction fit is ordinarily adequate.

With this electrode arrangement, the effects of sputtering become noticeable after several hours, if the exit window is mounted immediately below the anode. Since the base of the lamp must be mounted 12.5 cm from the excitation region, no light is lost when the exit window is moved 6 cm from the anode, to the end of a pipe, as shown in Fig. 8. Here the effects of sputtering are barely noticeable, even after 25 continuous hours of lamp operation. Complications such as self-reversal and reabsorption are not present, because the pipe does not contain molecules in the $1s\sigma 2p\sigma\ ^3\Sigma_u$ state. The exit window is a converging lens of 5.0-cm focal length, mounted in a removable threaded cap and made of Suprasil, the highest quality optical quartz available. An inferior grade of quartz, used in some of the tests, lost much of its ultraviolet transmission (i.e., became solarized) after prolonged exposure to the direct radiation from the arc.

The H_2 gas is prepurified, furnished in standard small cylinders. It enters just above the lens and is pumped through the lamp at a constant rate. The flow of gas entering the lamp is regulated by an adjustable bleeder valve (Vactronic VVB-50Q), usually set for a flow

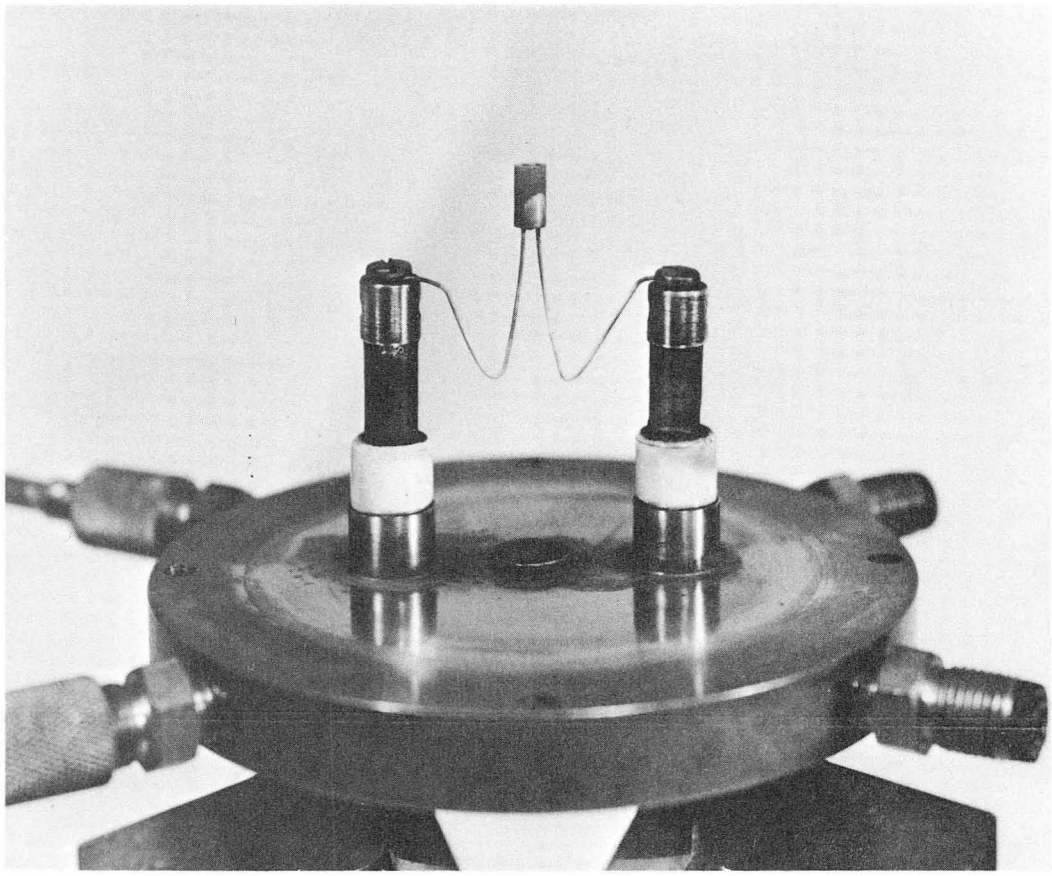

XBB 675-2607

Fig. 9. Photograph of lamp cathode and filament.

rate of about 0.2 cm^3/sec @ STP. The forepump is attached to the side of the lamp body, the pumping rate being controlled by a small gate valve. No diffusion pump is used. Two pressure gauges monitor the pressure within the lamp, a thermocouple gauge calibrated for air, useful primarily as a pre-run check for leaks, and a Wallace-Tiernan FA160 absolute-pressure gauge for measurement of the H_2 pressure during lamp operation. Its linear scale reads from 0.1 to 20.0 Torr. The adjustable valves are easily set for constant pressure. Pressures below 1.0 Torr result in less than the maximum intensity of ultraviolet radiation. Below 0.2 Torr, the lamp may emit radio-frequency radiation, which can be picked up by the counting circuits. Above 5.0 Torr, the intensity falls off because the discharge becomes unstable and confined to one side of the cathode, usually the side closest to the inner wall of the anode. Between 2.0 and 2.5 Torr the maximum 2275Å intensity is attained. The discharge is distributed uniformly throughout the region surrounding the cathode, and appears uniform even if the cathode's position is not quite concentric within the anode. Pressure drift is negligible, less than 0.1 Torr during a 25-hour run. The lamp can be run unattended.

Power for the lamp is taken from the 120-volt laboratory d.c. generator. The positive side (common) is grounded to the lamp body, and the negative side connects to the cathode through an adjustable 5- to 9-ohm ballast resistor, which limits the current to between 10 and 20 amperes. The voltage across the lamp depends on the H_2 pressure, but is nearly independent of the current. With a pressure of 2.0 Torr, this potential difference is about 30 volts, so that a typical power dissipation for the lamp is 500 watts.

The 2275Å interference filter, 1.3 cm in diameter, is mounted in the threaded cap which holds the Suprasil lens. The filter has a Suprasil substrate and is of the multilayer type, made by Thin Film Products, Inc. It represents the best effort of present-day technology. The transmission spectrum is asymmetric, having a maximum transmission of 23% at 2250Å and 12%-transmission points at 2130Å and 2450Å. In the visible region the transmission is 0.1% or less. This filter is contained within the main vacuum chamber, and is of a design intended to withstand the pressure shock of pumping.

A useful fluorescent screen is a metal strip painted with a paste of sodium salicylate in methyl alcohol. This screen emits a bright blue glow in the presence of ultraviolet radiation, and permits the path of the focused light to be traced. When a Pyrex plate is held over the lamp's exit window, the radiation is absorbed and the glow disappears completely. A cadmium sulfide cell coated with the fluorescent paste is installed within the main chamber to monitor the relative intensity of the lamp during the progress of a run.

If the H_2 pressure and d.c. current remain constant, the intensity falls off by about 10% in 25 hours. (If desired, compensation can be achieved by an adjustment of the ballast resistor.) The gradual loss of intensity is due to sputtering, which results in the deposit of a thin metallic layer on the surface of the lens. Before each run the lens is removed for cleaning with dilute HCl, scouring with steel wool, and a final cleaning with acetone. This procedure restores the lamp output. The anode and the quartz insulating plate (Fig. 8) are cleaned in the same way; during lamp operation they acquire a shiny, dark deposit,

probably originating from the cathode. In spite of this loss of cathode material, the cathode most recently in use has withstood more than 60 hours of operation (two runs of the experiment) with no apparent loss in discharge intensity or ease of starting. These cathodes can be exposed to air during installation and cleaning, without noticeable poisoning. No activation is necessary.

Development of the lamp included some experimentation with external heating of the cathode by means of a continuous current through the filament wire. Although a slight increase in intensity can be obtained in this way (up to 15%), the cathode life is shortened and the sputtering rate is as much as four times the rate for an unheated filament. A considerably lower cathode temperature, achieved by removal of heat through a larger-diameter support wire (0.13 cm), led only to loss of intensity. The optimum wire diameter is about 0.09 cm for the geometry shown in Fig. 8.

The temporary substitution of D_2 for H_2 made only a small improvement in the ultraviolet intensity. H_2 was used in all of the final runs of the experiment.

An estimate of the absolute intensity was made with a radiation thermopile (Reeder thermocouple RP-3M-3) fitted with a CaF_2 window and having a sensitive area 6×10^{-3} cm^2. Its rated sensitivity is 12 μvolts/μwatt. The manufacturer states that the sensitivity is uniform between 2000Å and 80,000Å. After passing through the focusing lens and interference filter, the radiation beam converges to a crude focus near the axis of the excitation chamber. A 0.8-cm diameter baffle, shown in Fig. 4, serves to cut off the flare surrounding the

beam of excitation radiation. If allowed to enter the photomultipliers, the light in this flare would increase the background counting rates. With the baffle in place and the thermocouple receiver positioned at the excitation region, the output voltage is 30 μvolts when the lamp current is 15 amperes. The intensity falls off to 15 μvolts near the edge of the beam. The average intensity at this region is therefore about 3×10^2 μwatt/cm^2. This estimate was quoted earlier in Section IV.

The measured voltage drops to less than 0.1 μvolt when a plastic or Pyrex plate is inserted into the path of the radiation, but only to 20 μvolts when a sheet of quartz is inserted. These results serve as evidence that the thermopile is responding to ultraviolet radiation, rather than to visible or infrared.

The measured intensity 3×10^2 μwatt/cm^2 for a 300Å band implies a photon flux of 10^{12} photons/(sec·cm^2·Å) at 2300Å. This is the flux at the excitation region, after the lens, filter, and baffle, and with the obvious solid-angle loss. The lamp described by Hartman [H-4] is claimed to emit 3×10^8 photons/(sec·cm^2·Å) at 1930Å. However, quantitative comparison is difficult, because Hartman used an exit slit of unspecified width.

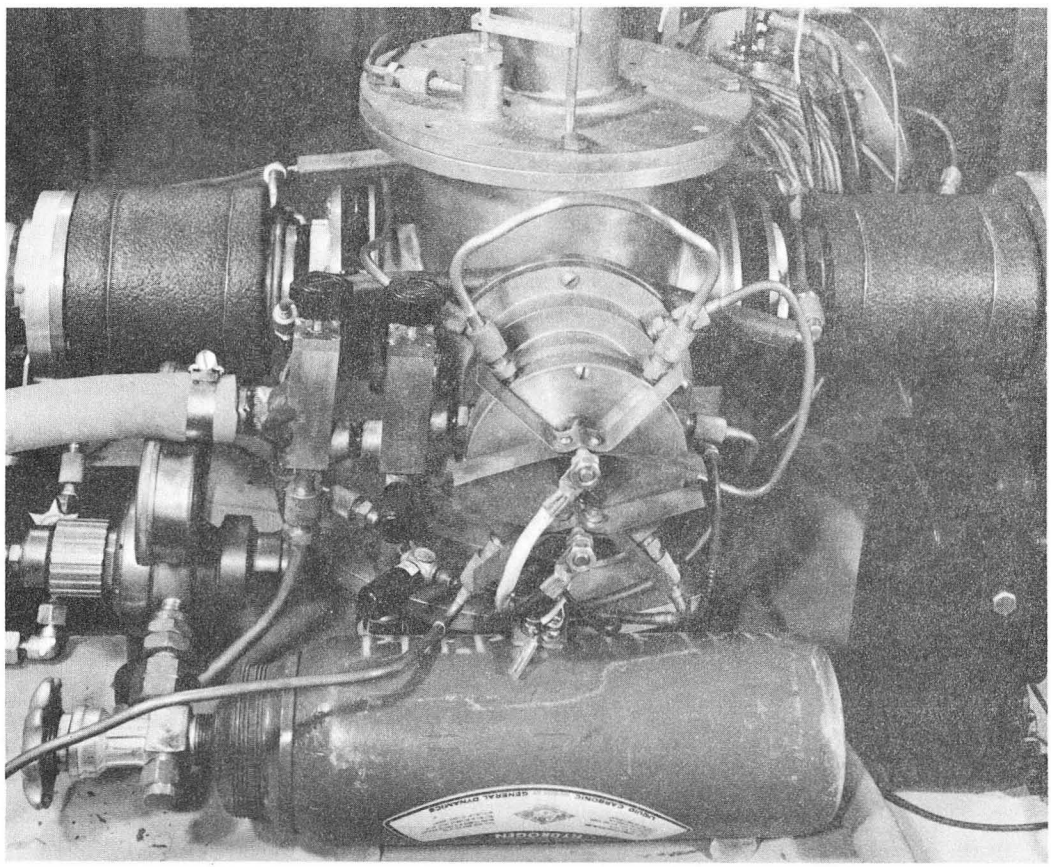

XBB 675-2609

Fig. 10. H_2 lamp mounted on excitation chamber.

D. Photon Detectors

Each detector assembly consists of a lens, a linear polarizer, an interference filter, and a photomultiplier tube. The lenses have 8-cm focal lengths. Mounted within the excitation chamber, they serve to improve the effective solid angles subtended by the detectors and to assure approximately plane wavefronts as the light passes through the polarizer and filter.

Near the blue end of the visible spectrum, Polaroid polarizers provide incomplete polarization. A more suitable material for the present experiment, where quantum efficiency is critical, is Polacoat 105MB. It is made commercially by the application of an azo dye to a glass substrate whose surface has been rubbed with an abrasive to produce many very fine, parallel scratches [M-1]. Table II summarizes the relevant polarization characteristics, which will be used in a subsequent calculation. Circular plates of 105MB polarizer, 7 cm in diameter, are set in rotatable mounts outside the vacuum chamber (Fig. 4).

Great care must be taken to eliminate spurious photomultiplier pulses. In this experiment the background rates are determined not primarily by photomultiplier dark noise, but by stray visible light reaching the photocathodes. This visible light is too dim to be seen with the naked eye, even in a dark room. Its source is blackbody radiation from the oven and wall fluorescence due to ultraviolet H_2 radiation. The H_2 lamp emits no detectable visible radiation; the lamp's effect on the pulse rates disappears when it is covered by a Pyrex plate. Carefully placed baffles help to decrease the scattering of visible light within the excitation chamber. To reduce further the

TABLE II. Characteristics of Polacoat 105MB linear polarizer

Wavelength	P_s	$P_{\|}$	$P_{\perp}$	α	β
λ_1 = 5513Å	0.46	0.32	0.05	0.80	0.06
λ_2 = 4227Å	0.42	0.27	0.05	0.75	0.06

Definitions:

α = Prob. of transmission of $|x\rangle$ photon by polarizer, axis along x.

β = Prob. of transmission of $|x\rangle$ photon by polarizer, axis along y.

P_s = Prob. of transmission of unpol. light by single sheet of polarizer.

$P_{\|}$ = Prob. of transmission of unpol. light by 2 sheets, axes $\|$.

$P_{\perp}$ = Prob. of transmission of unpol. light by 2 sheets, axes $\perp$.

$$P_s = \frac{1}{2}(\alpha + \beta);\ P_{\|} = \frac{1}{2}(\alpha^2 + \beta^2);\ P_{\perp} = \alpha\beta.$$

The expected relation $P_s^2 = \frac{1}{2}(P_{\|} + P_{\perp})$ is not satisfied in practice because reflections were not taken into account.

Transmission measurements were made on a Beckman DK-1A spectrophotometer.

fluorescence and scattering effects, the baffles and interior surfaces of the excitation chamber are painted with Aquadag and then blackened with soot deposited from a propane flame. These precautions are necessary, but not nearly sufficient to reduce the background rates to an acceptably low rate. Narrow-band interference filters make the crucial difference.

The filters for γ_1 and γ_2 were built specifically for peak transmission at the wavelengths $\lambda_1 = 5513\text{Å}$ and $\lambda_2 = 4227\text{Å}$, respectively. Their transmission characteristics are listed in Table III. Broadband filters ($\Delta\lambda \approx 150\text{Å}$) were used in the initial attempts, but they transmitted an intolerable background of scattered light. This light has a continuous spectrum. Therefore, if the filters provide complete rejection of wavelengths far from the peak, the background counting rates will be proportional to the filter bandwidths. Narrow-band filters have recently been developed which offer excellent blocking, high peak transmission (about 45%), and bandwidths as narrow as 2Å. The filters in Table III reduce the background to about 10^3 photons/sec in each detector. These rates are determined experimentally from the measured pulse rates and a knowledge of the quantum efficiencies of the photomultipliers. They are sufficiently low that it is worthwhile to cool the photocathodes. The tubes are cooled to -5° C by a Freon-12 refrigerator whose evaporator consists of copper tubing soldered to the photomultiplier mounts. Dry nitrogen gas is passed through the detector assemblies to prevent condensation of water vapor on the cold glass surfaces.

The photomultipliers have cathodes 5 cm in diameter, and are chosen for high quantum efficiency, low dark noise, and good time

TABLE III. Characteristics of interference filters for photon detectors

	#1	#2
Wavelength of max. transmission	5513Å	4227Å
FWHM $\Delta\lambda$	17Å	4.2Å
Peak transmission T	47%	43%
Blocking trans.	0.01% to 0.1%	0.01% to 0.1%
Temperature coeff.	0.18Å/degree C	0.18Å/degree C
Manufacturer	Spectrolab	Thin Film Products

resolution. Photomultiplier No. 1 (RCA type 7265) has 14 stages and an S-20 cathode, with a quantum efficiency $Q \approx 10\%$ at 5513Å; No. 2 (RCA type 8575) has 12 stages and a bialkali cathode, with $Q \approx 20\%$ at 4227Å.

Several tubes of each type (and of other types) were compared in a testing chamber, where the photocathode could be illuminated by a very low-intensity light source consisting of a lamp, an optical attenuator (layers of drafting tape), and an interference filter peaked at the desired wavelength. The attenuation was adjusted for a photon pulse counting rate between 10^3 and 10^4/sec, measured with the pulse counters described in Part E. The dynode resistors are wired according to a standard low-current circuit; the focusing-electrode voltage is adjustable for maximum signal. It is possible to count virtually all of the single-photoelectron pulses. In practice the counting rate is found to be almost independent of the anode voltage, remaining constant to within 10% from 1800 to 3000 volts, for example. The same incident photon flux was applied to all tubes tested. The pulse rate, with the dark rate subtracted, is proportional to the quantum efficiency.

Tubes having high dark noise were excluded. From the remainder, those having the highest quantum efficiency were selected. The time resolution, limited by the spread in electron transit times, is about 3 nsec (3×10^{-9} sec) for the 7265 and 2 nsec for the 8575. With typical anode voltages (2700 and 2200 volts, respectively), the two tubes have about the same multiplier gain, approximately 10^7. The gain is irrelevant, provided that the electronic circuits have sufficient sensitivity to respond to essentially all of the single-photoelectron pulses. The photomultipliers are provided with magnetic

and radio-frequency shielding.

The overall efficiency η of each detector is $\eta = QT\Omega/4\pi$, where T is the peak transmission of the interference filter and Ω is the solid angle subtended by the detector. For the geometry of Fig. 4, $\Omega = 0.28$ steradians. Thus $\eta_1 \cong 1 \times 10^{-3}$ and $\eta_2 \cong 2 \times 10^{-3}$. Imperfect focusing by the lenses will result in somewhat lower values. The approximate value $\eta \approx 10^{-3}$ was used in the coincidence-rate estimate made at the end of Section IV.

E. Electronics

The electronic circuits, indicated in Fig. 11, include provisions for time analysis and for conventional coincidence counting. Except for the pulse-height analyzer, all components were designed by the Lawrence Radiation Laboratory at Berkeley.

The negative output pulses from the photomultiplier anodes are amplified by 50-ohm wideband d.c. amplifiers, which provide 100X amplification for each detector. Because of the statistical nature of the electron multiplication process in the photomultipliers, the pulses have a wide range of amplitudes. The constant-delay discriminators convert these pulses into a sequence of uniform pulses, all of which have the same amplitude (-1 volt) and risetime (about 3 nsec). One of the important properties of this discriminator design is that its time delay does not vary appreciably with input pulse amplitude.

Three identical coincidence circuits and scalers, denoted by A, B, and C in Fig. 11, are operated simultaneously. Circuit B has no net delay in its inputs, and may be said to have "correct" timing. The cable lengths between the photomultiplier anodes and the wideband amplifiers are chosen so that circuit B will record a count when coincident flashes of light are received at the two detectors. The other two coincidence circuits, A and C, have long net delays inserted in their inputs #1 and #2, respectively. Counts recorded by A and C are "accidental" coincidences. They are a useful measure of the background counting rate. In all three coincidence circuits the clipping lines (RG-63, 125 ohms) are 1.0 meter in length. The corresponding resolving time (total width) is $2\tau = 16$ nsec. The

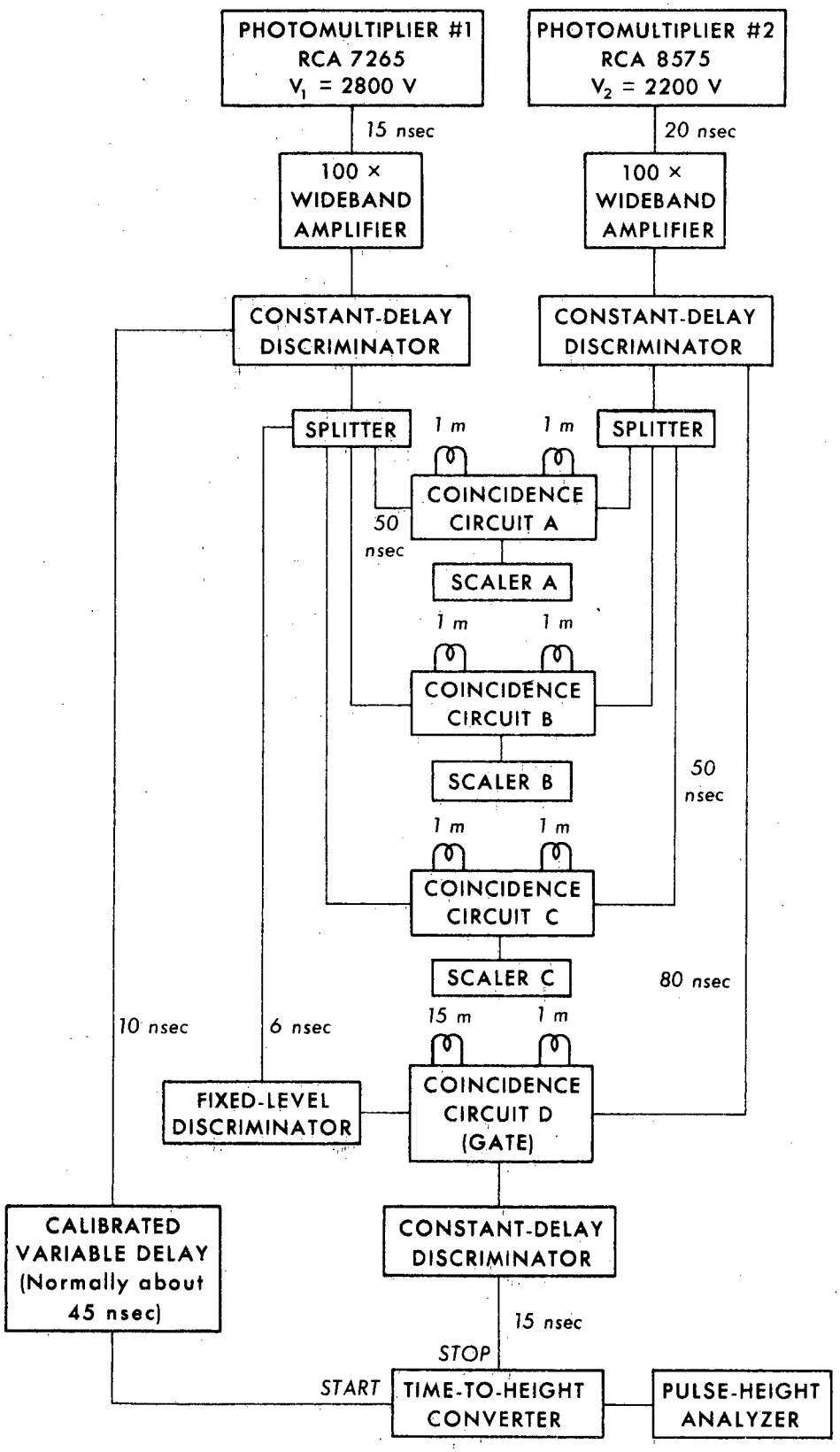

Fig. 11. Block diagram of electronics.

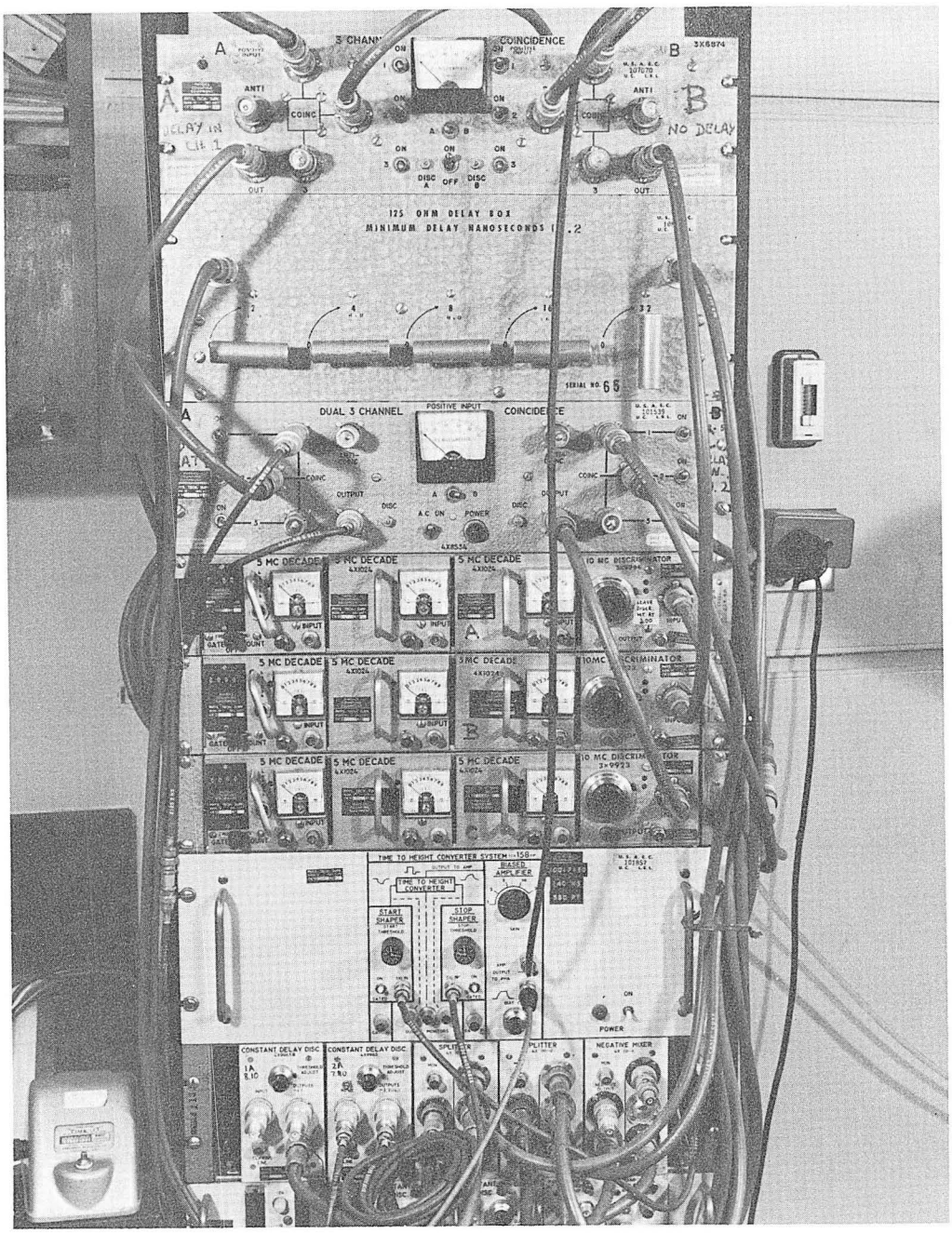

XBB 675-2604

Fig. 12. A portion of the main electronics rack. Shown from top to bottom are the calibrated variable delay, coincidence circuits, scalers, time-to-height converter, wide-band amplifiers and constant-delay discriminators.

discriminator thresholds on A, B, and C are set for equal coincidence counting rates when the detectors are exposed to light of low intensity (10^4 to 10^5 photons/sec at each photocathode). Normalization problems result from an ever-present slow drift in the threshold settings. This difficulty is not present when the correlation is observed by the time-to-height converter and pulse-height analyzer. The channels of the analyzer are analogous to individual coincidence circuits.

From the singles counting rates it is possible to infer that almost every single-photoelectron pulse is counted. The evidence for this conclusion is that when the photon flux into one of the detectors is held constant, the signal counting rate is almost independent of photomultiplier anode voltage, over a broad range corresponding to a factor of 10 in gain. In addition, the signal is almost independent of the threshold adjustment on the constant-delay discriminator. The probability is very small that a single-photoelectron pulse will be of such low amplitude that the discriminator will not respond.

The time-to-height converter produces an output pulse whose amplitude is proportional to the time interval between the arrival of the "start" pulse and the arrival of the "stop" pulse. Pulses due to correlated cascade photons γ_1, γ_2 will arrive at these inputs with a distribution in delay times whose shape depends on the time response of the instruments and on the exponential decay of the intermediate atomic state. The setting of the variable delay in the "start" input shifts the zero-reference in the time scale. The delay is adjusted so that γ_1,γ_2 pulse pairs provide an average output pulse amplitude which is about half the maximum amplitude available from the converter.

The maximum amplitude is about 8 volts and corresponds to a full-scale delay of about 120 nsec. Longer time intervals cannot be measured with this converter. Coincidence circuit D, shown in conjunction with a fixed-level discriminator and a constant-delay discriminator, serves as a gate which passes a "stop" pulse only when it follows a "start" pulse by less than 200 nsec. These components are necessary because the time-to-height converter would otherwise be affected by pulse pairs more than 240 nsec apart.

The pulse amplitude at the input of the analyzer determines the channel in which the count will be stored. The channel number is a linear function of the time delay between the γ_1 and γ_2 pulses. Two analyzers were employed at different times during the development of the experiment, a 400-channel RIDL model 24-2 and a 256-channel RCL model 20609. A subgroup of 100 or 128 channels is chosen to correspond to a time interval of about 100 nsec. The analyzer memory can be printed out or displayed on an oscilloscope screen. The horizontal and vertical axes correspond, respectively, to the channel number and the number of counts stored per channel. To calibrate the time scale, pulses from one of the photomultipliers are sent simultaneously into both wideband amplifiers, and the active analyzer channel is noted as a function of the calibrated delay setting.

The overall time response of the system, including both detectors as well as the electronics, can be measured by means of a radioactive source and a fast scintillator. A Co^{60} sample and a small block of Pilot scintillator B emit flashes of visible light having a duration of about 2 nsec [L-1]. This light source was mounted between the two

detector assemblies. Each flash of light is for practical purposes a delta-function input to the system. The time-correlated photomultiplier pulse pairs contribute to a peak in the analyzer display. The peaked curve, resembling a gaussian, has a full width at half-maximum of about 7 nsec, and is a good approximation to the Green's function for the system. After a small correction for the 2-nsec scintillator response, the width of the Green's function is 6 nsec. This figure includes contributions from the photomultipliers, constant-delay discriminators, time-to-height converter, and analyzer. When cascade photons are observed, the analyzer display will be a convolution of the Green's function and the decay curve for the intermediate atomic state. The lifetime of the 4^1P_1 state in calcium is about 4.5 nsec (less than the instrumental resolution), and therefore the shape of the decay curve cannot be accurately determined in this experiment.

The background counting rate $2\tau N_1 N_2$ depends on the resolving time 2τ of the coincidence circuit, or, equivalently, on the channel width for the analyzer. In each detector most of the counts recorded during a run are not due to cascade photons. In detector #1 most of the counts are attributable to stray light, and in #2 most are due to γ_2 photons not preceded by γ_1 photons. To a good approximation, therefore, N_1 and N_2 may be taken to be the total pulse rates from the individual detectors.

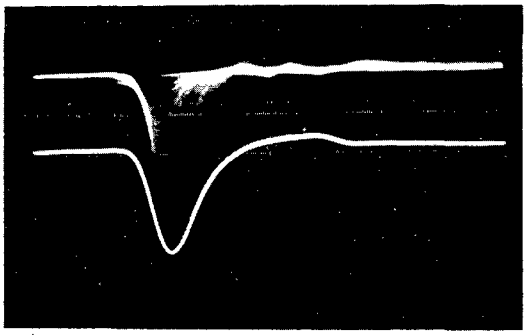

Fig. 13

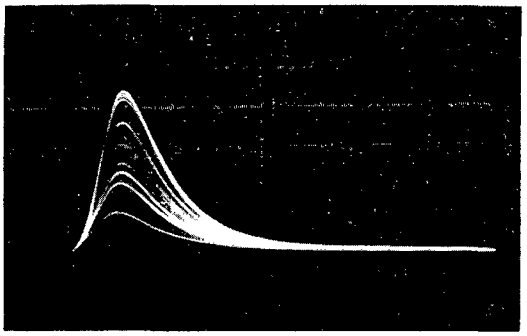

Fig. 14

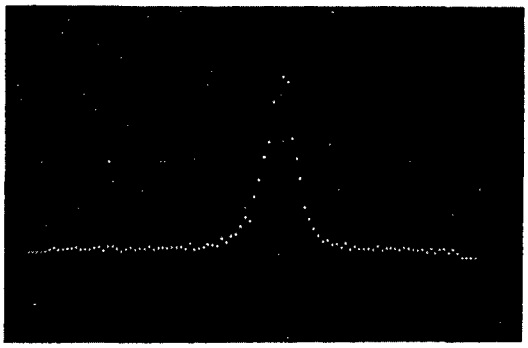

Fig. 15

XBB 675-2621

Fig. 13. Upper trace: Single-photoelectron pulses at photomultiplier anode (10 nsec/cm). Lower trace: Output of constant-delay discriminator (10 nsec/cm). (Techtronics 585A oscilloscope with Type 82 plug-in).

Fig. 14. Pulses from time-to-height converter (1.0 μsec/cm).

Fig. 15. Analyzer display of timing check with radioactive source and fast scintillator (1.0 nsec/channel).

VI. EXPERIMENTAL PROCEDURES; OBSERVED COUNTING RATES

Before any serious attempts to observe the polarization correlation, trial runs were undertaken with the polarizers removed. The purpose of these tests was to demonstrate that cascade photons could be counted and that a time correlation peak would be recorded by the analyzer.

Preparation for a run begins with cleaning of the lamp anode and exit window, cleaning of the beam oven, and loading with a 12-gm cylinder of calcium. The excitation and source chambers are evacuated, and the refrigerator is switched on. A special heater is provided for the 4227Å interference filter, which is mounted in a thermally insulated chamber. The heater current is adjusted to keep the filter at 20° C, as measured by a thermocouple in the filter mount. These precautions are necessary because the wavelength of maximum transmission shifts by about 2.1Å (the half-width) when the filter temperature drops 12°.

The beam oven is heated to its operating temperature, and then the H_2 lamp is turned on. The relative lamp output is monitored by the CdS detector (Section V, Part C). Ordinarily the drift in ultraviolet intensity is a negligible monotonic decrease of about 0.4% per hour. The calcium beam density, on the other hand, does fluctuate significantly, since a one-percent change in a.c. line voltage causes a somewhat larger change (perhaps 10%) in the observed excitation rate.

The best measure of the excitation rate R is the pulse counting rate N_2 for detector #2, which has an estimated efficiency $\eta_2 = 2 \times 10^{-3}$. Table IV shows representative counting rates for the individual detectors, and indicates the sources of noise. Of particular interest are the

TABLE IV. Typical pulse counting rates during a time-correlation test with polarizers removed

	H_2 Lamp	Ca Beam	N_1 (counts/sec)	N_2 (counts/sec)
Dark noise	off	off	150	120
Dark noise + fluorescence	on	off	220	150
Dark noise + oven light	off	on	370	250
Dark noise + fluorescence + oven light + signal	on	on	520	3380
Signal only, by subtraction			80	3100

Signal ratio: $\frac{N_1^{sig}}{N_2^{sig}} = \frac{80}{3100} = 2.6\%$

Conditions: Photomultipliers cooled to -5° C.

Ca beam density approximately $3 \times 10^{10}/cm^3$.

signal rates $N_1^{sig} = 80/sec$ and $N_2^{sig} = 3100/sec$. Thus, experimentally, $R \tilde{=} N_2/\eta_2 = 2 \times 10^6/sec$. In Section IV we predicted $R \approx 10^7/sec$.

The observed signal ratio is $N_1^{sig}/N_2^{sig} = 2.6\%$. The branching ratio for the transition $6^1P_1 \rightarrow 6^1S_0$, discussed in Section IV, should be η_2/η_1 (about 2) times the signal ratio, or about 5%. This value is less than the 25% branching ratio obtained by the Bates-Damgaard calculation. Excitation of the 5^1P_1 state can account for some of the difference. Probably most of it should be attributed to an inaccuracy in the Bates-Damgaard method, although the possibility remains that the detector efficiencies η are in error. In any case, the small signal ratio implies a coincidence rate lower than the estimate of Section IV. We expect that the coincidence rate $N_c = \eta_2 N_1^{sig}$ will be less than $10^{-1}/sec$.

If $\tau = 10^{-8}$ sec, the accidental coincidence rate $2\tau N_1 N_2$ will be about $3 \times 10^{-2}/sec$. Even if the signal and background rates are comparable, the time correlation can be distinguished without difficulty. In a complete run the total number of signal counts will be many times the standard deviation, which is the square root of the background and signal together.

In the time correlation run made on September 29 and 30, 1966, the total numbers of coincidence counts recorded by circuits A, B, and C (polarizers removed) were $n^A = 1964$, $n^B = 3437$, and $n^C = 1921$. The counters were read every 30 minutes. The oven was in operation for 16.5 hours; data were recorded during a shorter time t = 12 hours. By the end of the run, the analyzer had accumulated the correlation peak shown in Fig. 16. The asymmetry is due to the exponential decay of the 4^1P_1 state. In this run the photomultipliers were not cooled, and

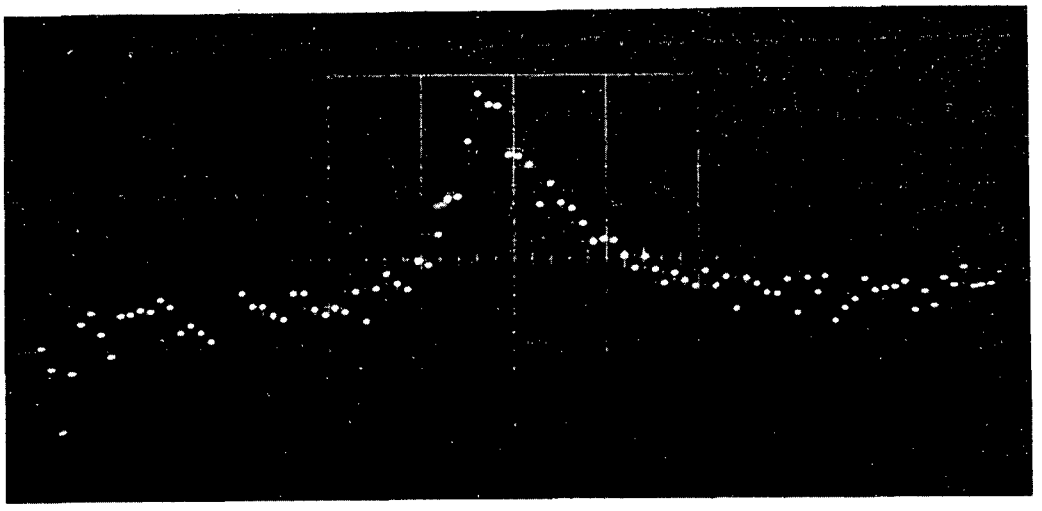

XBB 675-2623

Fig. 16. Time correlation, September 29 and 30, 1966, polarizers removed. (0.80 nsec/channel; full scale = 256 counts/channel). Note exponential decay of intermediate atomic state. Horizontal scale reference should not be compared with reference in Fig. 15.

the dark noise rates were correspondingly high. The average coincidence rate for cascade photon pairs was $N_c = \frac{1}{t}[n^B - \frac{1}{2}(n^A + n^C)] = 3.5 \times 10^{-2}$/sec, as measured by the coincidence circuits. Since their resolving time is shorter than the time-width of the analyzer peak, some coincidence counts are missed by circuit B. A more precise value of N_c can be obtained from the printed record of the analyzer memory. The counts recorded within the peak are summed, and the background rate is subtracted, leaving in this case a total of 1838 coincidence counts. By this method the average coincidence rate was $N_c = 4.3 \times 10^{-2}$/sec.

After this test had proved that correlated γ_1, γ_2 photon pairs could be detected, the linear polarizers were installed, in preparation for attempts to observe the polarization correlation.

When the lamp and beam oven are in operation, the singles rates vary insignificantly with polarizer orientation. The small variation observed is due to polarization of stray light reflected within the vacuum chamber. It contributes to all analyzer channels with equal probability.

VII. RESULTS AND DISCUSSION

Because the calcium beam density tended to fluctuate with the line voltage, measurements with the polarizer axes set parallel and perpendicular were made alternately. One polarizer was fixed, and the orientation of the other was changed by 90° every 15 minutes. Two sets of analyzer channels were used, one set for each orientation. Runs were made with different orientations of the fixed polarizer, and in each case the correlation was found to depend only on the relative angle between the axes. Figures 17 and 18 show the results of a 21-hour run, December 17 and 18, 1966. They indicate clearly the difference between the coincidence rates for parallel and perpendicular orientations.

The coincidence counts recorded by the counters are $n_{\parallel}^{A} = 477$; $n_{\perp}^{A} = 476$; $n_{\parallel}^{B} = 936$; $n_{\perp}^{B} = 569$; $n_{\parallel}^{C} = 442$; $n_{\perp}^{C} = 475$. The numbers of signal counts, taken directly from the analyzer memory, are approximately $n_{\parallel}^{sig} = 490$ and $n_{\perp}^{sig} = 70$. Thus $n_{\perp}^{sig}/n_{\parallel}^{sig} = 70/490 = 0.14$. The nonzero value of this ratio can be attributed entirely to the incomplete polarization of the Polacoat 105MB polarizers. To substantiate this claim, we must show how the values of α and β given in Table II (Section V, Part D) are related to the experimental values of the coincidence probabilities $P_{\parallel}$ and $P_{\perp}$. The photon state is $|\psi\rangle = \frac{1}{\sqrt{2}}[|x_1x_2\rangle - |y_1y_2\rangle]$ (Section II), where $|x\rangle$ and $|y\rangle$ are base states of linear polarization. Let $|X\rangle$ and $|Y\rangle$ refer to the polarizer orientations. Then $\alpha = |\langle X|x\rangle|^2 = |\langle Y|y\rangle|^2$ and $\beta = |\langle X|y\rangle|^2 = |\langle Y|x\rangle|^2$.

$$P_{\parallel} = |\langle X_1X_2|\psi\rangle|^2 = \tfrac{1}{2}[|\langle X_1X_2|x_1x_2\rangle|^2 + |\langle X_1X_2|y_1y_2\rangle|^2]$$

$$= \tfrac{1}{2}[\alpha_1\alpha_2 + \beta_1\beta_2] = \tfrac{1}{2}[(0.80)(0.75) + (0.06)^2] = 0.30$$

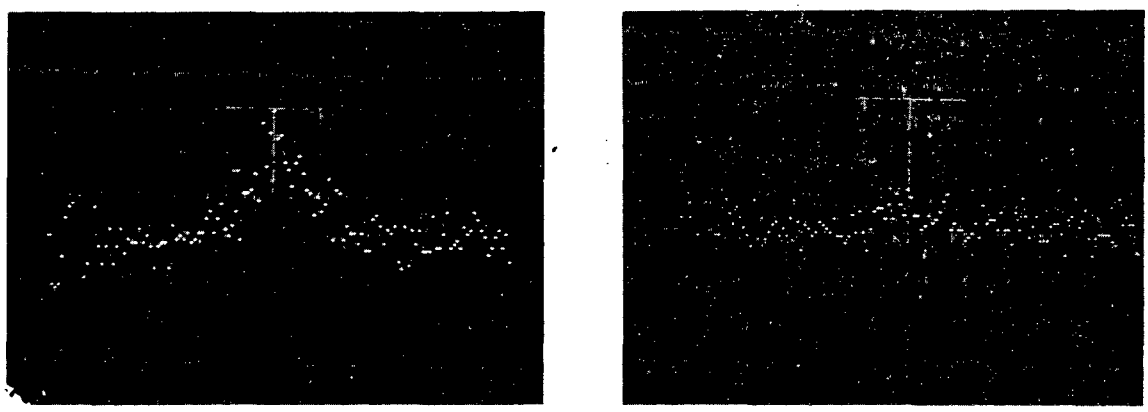

(a) (b)

XBB 675-2622

Fig. 17. Analyzer display showing results from polarization correlation experiment, December 17 and 18, 1966. (0.80 nsec/channel; full scale = 52 counts/channel). (a) Polarizer axes parallel; (b) Polarizer axes perpendicular.

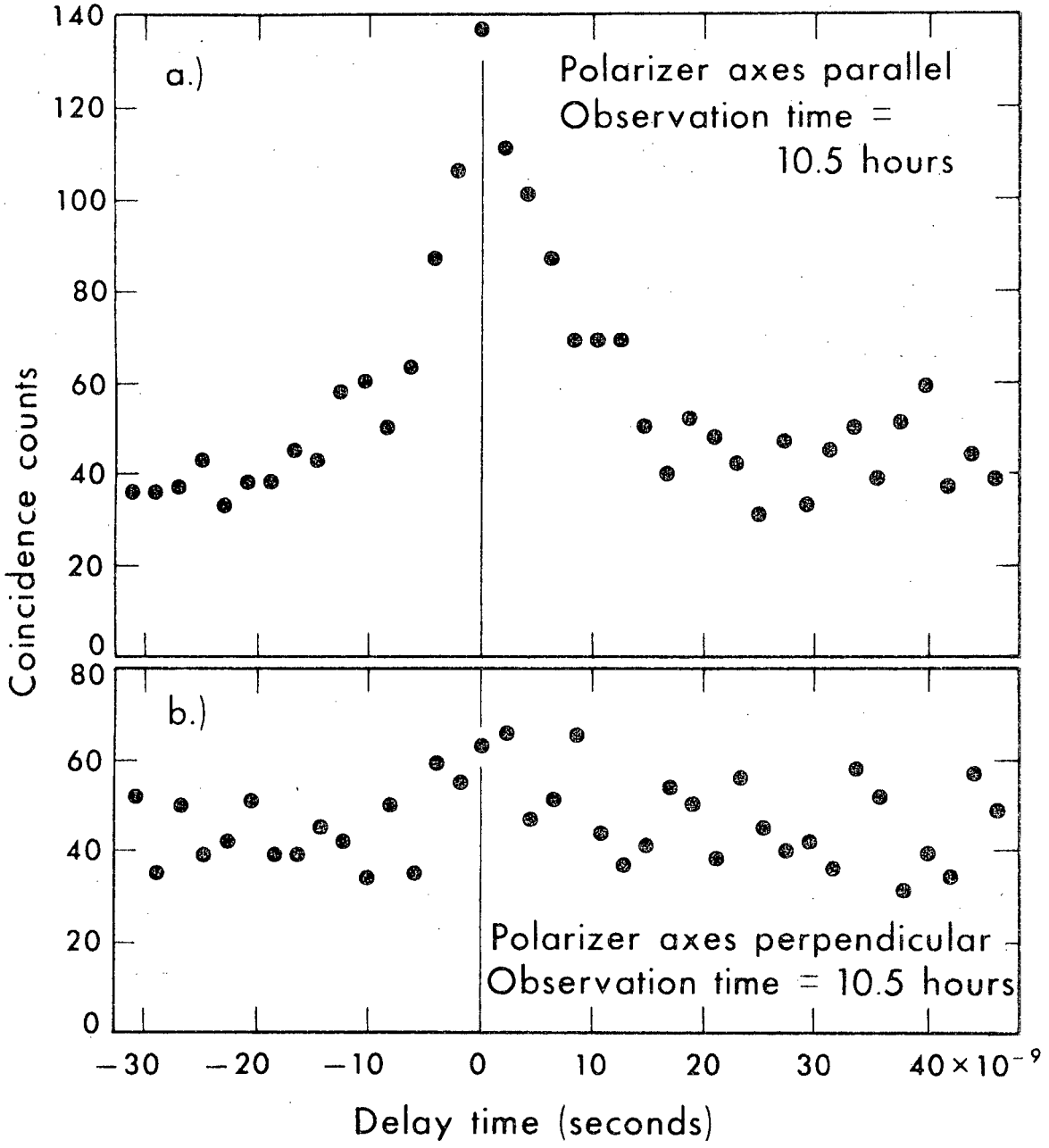

Fig. 18. Coincidence counts, as a function of relative time delay, showing polarization correlation. Each point represents a sum over three analyzer channels. Data were taken from printed record of analyzer memory. December 17 and 18, 1966.

$$P_{\perp} = |\langle X_1 Y_2 | \psi \rangle|^2 = \tfrac{1}{2}[|\langle X_1 Y_2 | x_1 x_2 \rangle|^2 + |\langle X_1 Y_2 | y_1 y_2 \rangle|^2]$$

$$= \tfrac{1}{2}[\alpha_1 \beta_2 + \beta_1 \alpha_2] = \tfrac{1}{2}[(0.80 + 0.75)(0.06)] = 0.046$$

$$\frac{P_{\perp}}{P_{\parallel}} = \frac{0.046}{0.30} = 0.15, \text{ in good agreement with the observed ratio } 0.14.$$

The experimental results are consistent with a coincidence probability of the form $P \sim \cos^2 \varphi$.

VIII. APPENDICES

APPENDIX A. SOME RELEVANT EXPERIMENTS

The present investigation is probably the first observation of photon polarization correlation in atomic spectrscopy. Similar problems have been pursued which involve correlations of radiations emitted by nuclei, most notably of gamma-rays in the MeV region. All of these experiments, directly or indirectly, are studies of the properties of many-particle quantum states.

One of the best known correlation experiments is the observation of the linear polarization correlation of the 0.5 MeV photon pairs emitted simultaneously in the annihilation of singlet positronium (Section II). The experimental verification, first proposed by Wheeler [W-2], was undertaken by several groups [B-7, H-3, H-6]. The greatest precision was achieved by Wu and Shaknov [W-5]. In that experiment, as in most nuclear cascade experiments, the linear polarizations are inferred from the azimuthal asymmetry in Compton scattering of the gamma-rays.

For several reasons, cascade experiments involving more than one polarization measurement are not ordinarily performed. One reason, discussed by Wightman [W-3], is that it is difficult to measure the polarization of MeV gamma-rays. Another is that although the determination of the relative parities of the nuclear states requires measurement of photon polarization, a single polarization measurement is sufficient if the angular correlation is also observed [H-1]. A search through the literature has turned up only one gamma-gamma linear polarization correlation experiment, by Robinson and Madansky in 1952 [R-4]. The most common type of correlation experiment involves the study of angular

correlations, without polarization measurement, and is useful in the determination of the angular momenta of nuclear states [B-6].

In the domain of atomic physics, the polarization of resonance fluorescence has been studied since the 1920's. Most of the relevant theory is described in the text by Heitler [H-5]. Quantum interference effects, observable in level crossings, are an interesting manifestation of photon correlations [C-3, K-2]. The technique of single photon counting has not been fully exploited in the visible region. A number of experiments have been proposed [A-2, B-12, B-13, C-1, S-1], but comparatively few have been performed. Noteworthy in the field of quantum optics is the study of Brown-Twiss correlations [M-3, for example]. Except for the present observations on calcium, most of the photon counting work in atomic physics has been confined to the ultraviolet region, where photomultiplier efficiencies can be high and the background rates comparatively low. Recently Kaul [K-1] succeeded in observing coincidences due to ultraviolet cascade photons in mercury, and applied time analysis to the measurement of the lifetime of a metastable state. Earlier, Brannen et al. [B-13] measured a lifetime in mercury by observation of a cascade in which the first transition originated from the ionization continuum. Lipeles, Novick, and Tolk [L-2] describe measurements of angular correlations in the two-photon decay $2s \rightarrow 1s$ in singly ionized helium, where the photon energy distributions are continuous and the observed wavelengths range from 300Å to 1200Å. In this region polarization measurements have been regarded as impractical.

Low counting rates are a serious obstacle to further applications of the techniques described in this paper. The presence of nuclear spin,

on the other hand, would result in only a partial loss of linear polarization correlation. If some means of excitation is found which permits the attainment of substantially higher counting rates, these methods may become useful in radio-frequency spectroscopic studies of the fine structure and hyperfine structure of excited atomic states.

APPENDIX B. THE EFFECT OF AN EXTERNAL MAGNETIC FIELD

An interesting question concerns the effect of an external magnetic field at the excitation region. The initial and final atomic states have zero magnetic moment, and are unaffected by the field. However, the intermediate state has a magnetic moment of one Bohr magneton, and in the presence of the field its sublevels show the usual Zeeman splitting. If the field is so large that the splitting exceeds the level width for the 4^1P_1 state, then the amplitudes for the states M = -1, 0, and +1 do not interfere, with the result that the polarization correlation is destroyed. In this case the Larmor period is much shorter than the natural lifetime of the state. The Larmor precession can be observed directly, as it affects the correlation in the times at which the cascade photons are detected. Effects of this type have been studied in nuclear angular correlation experiments [F-3, H-7].

The interaction Hamiltonian for the applied field is $H'' = \omega J_z$, where $\omega = \frac{eB}{2mc}$ is the Larmor frequency and where the z-axis is parallel to the direction of the field $\vec{B}$. This interaction does not mix the states in the sense that the off-diagonal matrix elements $\langle M_1|H''|M_2\rangle$ are nonzero, but it does affect the phases of the probability amplitudes for the three intermediate states. The intermediate state

$$\sum_M a_M|M\rangle$$

has amplitudes a_M which have a time dependence due to H", given by the Schrödinger equation

$$H''\Big(\sum_M a_M|M\rangle\Big) = i\hbar\frac{\partial}{\partial t}\Big(\sum_M a_M|M\rangle\Big).$$

It follows immediately that the amplitudes are $a_M(t) = a_M(0)\, e^{-iM\omega t}$ $\sim \langle 1M|\hat{\epsilon}_1\cdot\vec{r}|00\rangle\, e^{-iM\omega t}$. The final-state amplitude a_f now depends on the time t spent in the intermediate state.

$$a_f \sim \sum_M \langle 00|\hat{\epsilon}_2\cdot\vec{r}|1M\rangle\langle 1M|\hat{\epsilon}_1\cdot\vec{r}|00\rangle\, e^{-iM\omega t} \sim \sum_M (-1)^M \epsilon_{1\,-M}\epsilon_{2\,-M}\, e^{-iM\omega t}$$

Two geometrical arrangements are of particular interest, and are illustrated in Fig. 19. In case #1 the photons are observed along the z-axis, and in case #2 they are observed along an axis perpendicular to z.

The spherical components of the vector $\hat{\epsilon}$ are

$$\epsilon^{\pm 1} = \mp\frac{1}{\sqrt{2}}(\epsilon_x \pm i\epsilon_y)$$

and $\epsilon^0 = \epsilon_z$. The transversality conditions $\hat{\epsilon}\cdot\vec{k} = 0$ imply that $\epsilon_{1_z} = \epsilon_{2_z} = 0$ in case #1 and that $\epsilon_{1_y} = \epsilon_{2_y} = 0$ in case #2.

<u>Case #1</u>: $a_f \sim \frac{1}{2}(\epsilon_{1_x} + i\epsilon_{1_y})(\epsilon_{2_x} - i\epsilon_{2_y})e^{i\omega t} + \frac{1}{2}(\epsilon_{1_x} - i\epsilon_{1_y})(\epsilon_{2_x} + i\epsilon_{2_y})e^{-i\omega t}$

$$= \frac{1}{2}e^{i\varphi_1}e^{-i\varphi_2}e^{i\omega t} + \frac{1}{2}e^{-i\varphi_1}e^{i\varphi_2}e^{-i\omega t} = \cos(\varphi_2 - \varphi_1 - \omega t),$$

where φ_1 and φ_2 are the usual azimuthal angles of polarizer axes #1 and #2, measured with respect to the x-axis. If $\varphi \equiv \varphi_2 - \varphi_1$, the coincidence probability is $P = \frac{1}{2}\cos^2(\varphi - \omega t)$. The classical Larmor precession takes place in the xy-plane. A simple interpretation of this expression for the coincidence probability is that the atom precesses through an angle (ωt) between the emission of γ_1 and the emission of γ_2. If the

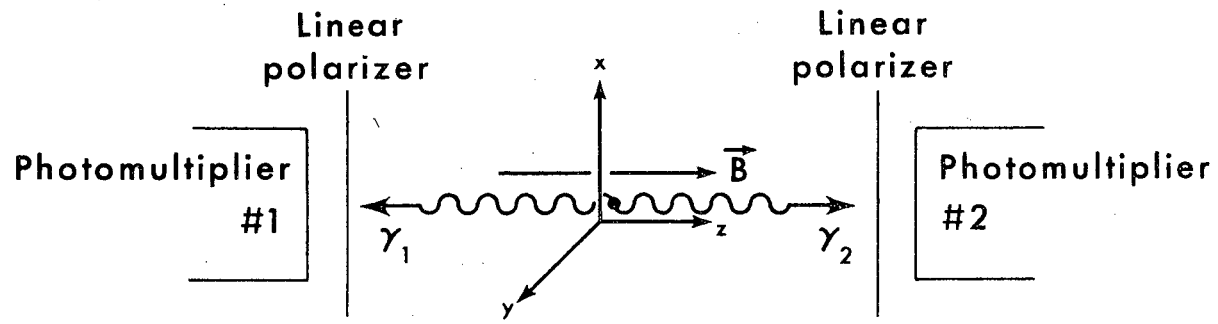

CASE 1: Observation axis parallel to $\vec{B}$

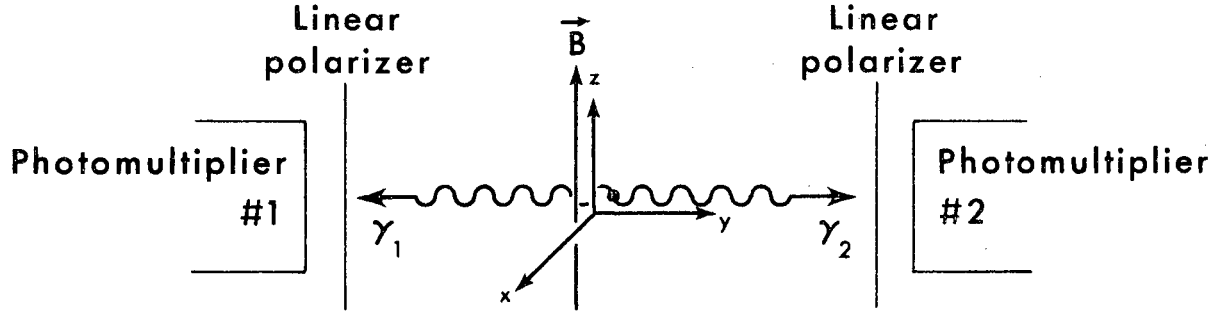

CASE 2: Observation axis perpendicular to $\vec{B}$

Fig. 19. Magnetic field experiments.

polarizer axes are parallel, then the probability $P = \frac{1}{2}\cos^2 \omega t$ is expected to modulate the exponential decay $e^{-t/\tau}$ for the intermediate state of the cascade. The magnetic field strength should be chosen for a Larmor period $2\pi/\omega$ of the order of twice the lifetime τ.

Case #2: $a_f \sim \frac{1}{2}\epsilon_{1_x}\epsilon_{2_x} e^{i\omega t} + \epsilon_{1_z}\epsilon_{2_z} + \frac{1}{2}\epsilon_{1_x}\epsilon_{2_x} e^{-i\omega t}$

$$= \sin \varphi_1 \sin \varphi_2 \cos \omega t + \cos \varphi_1 \cos \varphi_2,$$

where φ_1 and φ_2 are measured from the z-axis.

$$P = \frac{1}{2}(\sin \varphi_1 \sin \varphi_2 \cos \omega t + \cos \varphi_1 \cos \varphi_2)^2.$$

Case 2a: $\varphi_1 = \frac{\pi}{4}$, $\varphi_2 = -\frac{\pi}{4}$.

$$P = \frac{1}{8}(1 - \cos \omega t)^2 = \frac{1}{2}\sin^4 \frac{\omega t}{2}.$$

Case 2b: Polarizers are removed.

$$P = \frac{1}{2}\sum_{\substack{\text{unobserved} \\ \text{polarizations}}} (\sin \varphi_1 \sin \varphi_2 \cos \omega t + \cos \varphi_1 \cos \varphi_2)^2$$

$$= \frac{1}{2}(1 + \cos^2 \omega t)$$

This is the result obtained from the angular correlation $\frac{1}{2}(1 + \cos^2 \theta)$ when θ is replaced by $(\pi - \omega t)$, to account for the Larmor precession of the atom.

The natural lifetime of the 4^1P_1 state in calcium is so short that these effects are difficult to observe with the apparatus described in this paper. At best, the $(1 + \cos^2 \omega t)$ modulation will show up only at the first dip, where $\omega t = \frac{\pi}{2}$. An attempt was made to resolve the

precession in case 2b with a magnetic field B = 100 gauss. The time correlation shown in Fig. 20 is the result of this 34-hour run. The average coincidence rate was $N_c = 3.7 \times 10^{-2}$/sec. There appears to be a small porch at the expected location on the downward slope of the distribution. However, this result is inconclusive. Case #1 ($\varphi = \frac{\pi}{2}$) or case 2a might be more favorable. The run should be split into two sets of analyzer channels, for B = 0 and B > 100 gauss.

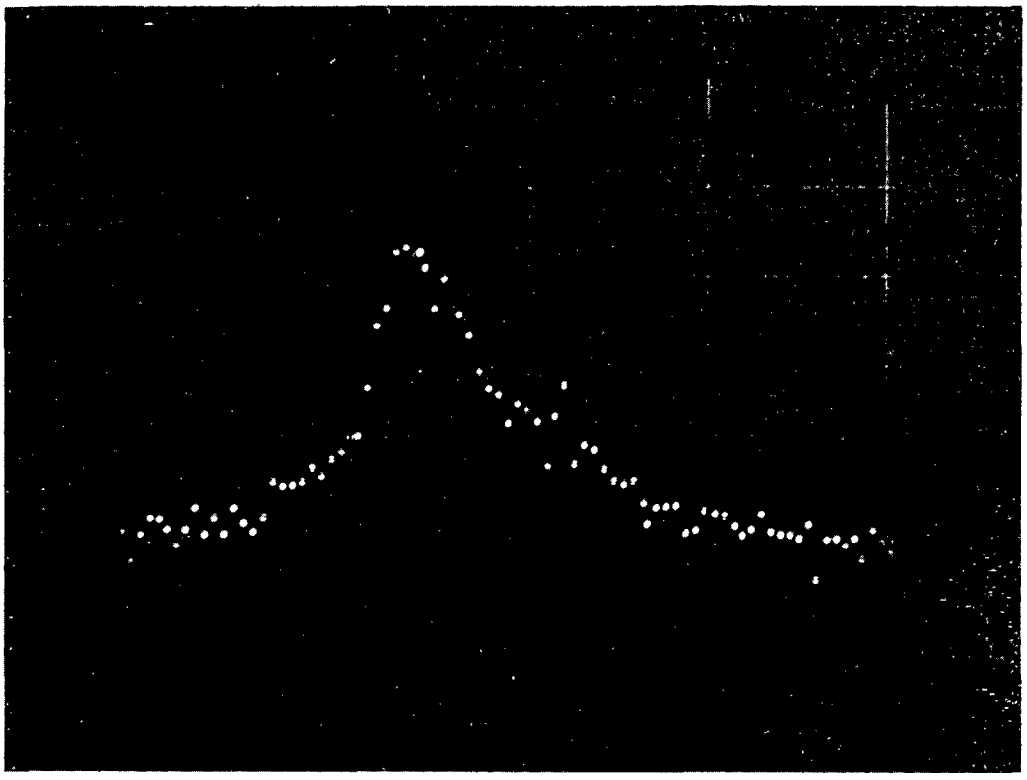

XBB 675-2687

Fig. 20. Time correlation, Case 2b, polarizers removed. B = 100 gauss. April 1, 2 and 3, 1967. (0.52 nsec/channel).

APPENDIX C. THE EINSTEIN-PODOLSKY-ROSEN PARADOX

The polarization correlation of cascade photons serves as a beautiful illustration of a well-known problem in the quantum theory of measurement, first described in 1935 by Einstein, Podolsky, and Rosen [E-1] and elucidated by Bohr [B-11]. In the calcium experiment each of the detected photon beams is unpolarized, since the orientations of the 4^1P_1 states are random. Consequently, the transmission probability is one-half for either of the linear polarizers, irrespective of its orientation. Einstein, Podolsky, and Rosen would attempt to describe the photon pair as "two systems." They reason as follows: "since at the time of measurement the two systems no longer interact, no real change can take place in the second system in consequence of anything that may be done to the first system." [E-1]. This assertion implies that the polarization measurements on the two photons are independent, and that the coincidence probability should be independent of the orientation of the polarizers.

The conflict between this apparently reasonable conclusion and the correlation predicted by quantum theory has been discussed in various contexts [B-4, B-8, B-9, F-4, I-1]. Although it is generally agreed that the usual interpretation of quantum theory is sufficient to explain correlation experiments, some authors have attempted to restore the classical notion of causality through the introduction of "hidden variables." This idea is still the subject of some speculation [B-5, B-10]. However, it may well be argued that a hidden variable model contributes little to our understanding of nature if the new theory cannot be distinguished experimentally from standard quantum theory.

Furry [F-4] has explored the consequences of the assumption that a particle belonging to a composite system has independent reality. Taking the present experiment as an example, Furry would suppose that the polarization states of γ_1 and γ_2 are definite. A correlation in linear polarization would be observed if the photons from each atom were linearly polarized in the same direction. All polarization directions would be equally probable, perhaps determined by some sort of hidden variable. Unfortunately, this linear polarization would preclude a correlation in circular polarization. Bohm and Aharonov [B-9], considering the case of positronium annihilation, point out that Furry's assumption is inconsistent with the experimental result of Wu and Shaknov [W-5].

The calcium cascade experiment may be examined from the point of view of such an assumption. This treatment is included here, not because it has any relevance to physics, but because it answers a question which has been raised on several occasions. As usual, let φ be the angle between the polarizer axes, and let ψ be the angle between the axis of polarizer #1 and the polarization direction for the photon pair. The transmission probabilities are $P_1 = \cos^2 \psi$ for γ_1 and $P_2 = \cos^2 (\psi + \varphi)$ for γ_2. The coincidence probability is $P = P_1 P_2$ for a given value of ψ. The angles ψ must be distributed uniformly between 0 and π. Thus, on average,

$$P = \frac{1}{\pi}\int_0^{\pi} \cos^2 \psi \cos^2 (\psi + \varphi)\, d\psi = \frac{1}{8} (1 + 2 \cos^2 \varphi).$$

This "correlation function" resembles the result from quantum theory, $\frac{1}{2} \cos^2 \varphi$. However, its maximum and minimum values are $\frac{3}{8}$ and $\frac{1}{8}$, instead

of $\frac{1}{2}$ and 0. If Furry's model were meaningful, $P_{\perp}/P_{\parallel} = \frac{1}{3}$ (perfect polarizers), whereas the experimental ratio is close to zero, in agreement with quantum theory.

The paradox of Einstein, Podolsky, and Rosen arises from a disparity between a formal theory and the authors' intuitive sense. Einstein said of Bohr's interpretation, "To believe this is logically possible without contradiction, but it is so very contrary to my scientific instinct that I cannot forego the search for a more complete conception." [S-2]. The search must continue, but it should be recognized that the common-sense intuition cannot always be trusted to furnish a useful mental picture of phenomena which lie outside the domain of experience.

IX. ACKNOWLEDGMENTS

I welcome this opportunity to thank Professor Eugene D. Commins, an exemplary research adviser and an outstanding teacher. His wise guidance and constant encouragement are acknowledged with gratitude.

I am greatly indebted to Professor Eyvind H. Wichmann for suggesting this experiment and for many useful discussions.

I wish to express my appreciation to Dr. David T. Phillips for much help with the electronics.

I would like to extend my thanks in general to the faculty of the Physics Department for invaluable advice on innumerable occasions, and to the staff of the Lawrence Radiation Laboratory for technical assistance and equipment.

I am grateful to the National Science Foundation for four years of fellowship support.

This work was supported in part by the U. S. Atomic Energy Commission and the Alfred P. Sloan Foundation.

X. REFERENCES

A-1 A. J. Allen, J. Opt. Soc. Am. 31, 268 (1941).

A-2 O. Aminian, Compt. Rend. (Paris) 255, 486 (1962).

B-1 J. P. Barrat, J. Phys. Radium 20, 541 and 633 (1959).

B-2 D. R. Bates and A. Damgaard, Phil. Trans. Roy. Soc. (London) Ser. A 242, 101 (1949).

B-3 W. A. Baum and L. Dunkelman, J. Opt. Soc. Am. 40, 782 (1950).

B-4 J. S. Bell, Physics 1, 195 (1964).

B-5 J. S. Bell, Rev. Mod. Phys. 38, 447 (1966).

B-6 L. C. Biedenharn and M. E. Rose, Rev. Mod. Phys. 25, 729 (1953).

B-7 E. Bleuler and H. L. Bradt, Phys. Rev. 73, 1398 (1948).

B-8 D. Bohm, Quantum Theory (Prentice-Hall, New York, 1951), Chap. 22.

B-9 D. Bohm and Y. Aharonov, Phys. Rev. 108, 1070 (1957).

B-10 D. Bohm and J. Bub, Rev. Mod. Phys. 38, 453 and 470 (1966).

B-11 N. Bohr, Phys. Rev. 48, 696 (1935).

B-12 L. C. Bradley, Phys. Rev. 102, 293 (1956).

B-13 E. Brannen, F. R. Hunt, R. H. Adlington, and R. W. Nicholls, Nature 175, 810 (1955).

B-14 B. Budick, R. Novick, and A. Lurio, Applied Optics 4, 229 (1965).

C-1 C. Camhy and A. M. Dumont, Ann. Astrophys. (Paris) 28, 113 (1965).

C-2 D. Chalonge, Ann. Phys. (Paris) Ser. 11, 1, 123 (1934).

C-3 F. D. Colegrove, P. A. Franken, R. R. Lewis, and R. H. Sands, Phys. Rev. Letters 3, 420 (1959).

C-4 A. S. Coolidge, Phys. Rev. 65, 236 (1944).

C-5 E. U. Condon and G. H. Shortley, The Theory of Atomic Spectra

(Cambridge University Press, 1935, 1963), Sec. 10^{4}.

E-1 A. Einstein, B. Podolsky, and N. Rosen, Phys. Rev. 47, 777 (1935).

F-1 R. P. Feynman, R. B. Leighton, and M. Sands, The Feynman Lectures on Physics (Addison-Wesley, 1965), Vol. III, Sec. 18-3.

F-2 N. A. Finkelstein, Rev. Sci. Instr. 21 509 (1950).

F-3 H. Frauenfelder and R. M. Steffen, in Alpha-, Beta- and Gamma-Ray Spectroscopy, edited by K. Siegbahn (North-Holland, Amsterdam, 1965), Vol. II, Chap. XIX.

F-4 W. H. Furry, Phys. Rev. 49, 393 (1936).

G-1 A. Gallagher, Private communication.

G-2 B. M. Glennon and W. L. Wiese, Bibliography on Atomic Transition Probabilities, National Bureau of Standards Misc. Publ. 278 (1966).

H-1 D. R. Hamilton, Phys. Rev. 74, 782 (1948).

H-2 Handbook of Chemistry and Physics (Chemical Rubber, 1963), 44th ed., p. 454.

H-3 R. C. Hanna, Nature 162, 332 (1948).

H-4 P. L. Hartman, J. Opt. Soc. Am. 51, 113 (1961).

H-5 W. Heitler, The Quantum Theory of Radiation, 3rd ed. (Clarendon Press, Oxford, 1954), Chap. 5.

H-6 F. L. Hereford, Phys. Rev. 81, 482 (1951).

H-7 A. Z. Hrynkiewicz, Nucl. Instr. Meth. 16, 317 (1962).

H-8 A. W. Hull, Phys. Rev. 56,86 (1939).

I-1 D. R. Inglis, Rev. Mod.Phys. 33, 1 (1961).

J-1 H. M. James and A. S. Coolidge, Phys. Rev. 55, 184 (1939).

K-1 R. D. Kaul, J. Opt. Soc. Am. 56, 1262 (1966).

K-2 B. P. Kibble and S. Pancharatnam, Proc. Phys. Soc. (London) 86, 1351 (1965).

K-3 C. A. Kocher and E. D. Commins, Phys. Rev. Letters 18, 575 (1967).

K-4 L. R. Koller, Ultraviolet Radiation (Wiley, New York, 1952), p. 74.

L-1 Lawrence Radiation Laboratory Counting Handbook UCRL-3307, Rev. 3 (Berkeley, 1966).

L-2 M. Lipeles, R. Novick, and N. Tolk, Phys. Rev. Letters 15, 690 (1965).

L-3 S. I. Levikov and L. P. Shishatskaya, Opt. Spectry. (USSR) 11, 371 (1961).

L-4 A. Lurio, R. L. de Zafra, and R. J. Goshen, Phys. Rev. 134, A1198 (1964).

M-1 M. N. McDermott and R. Novick, J. Opt. Soc. Am. 51, 1008 (1961).

M-2 C. E. Moore, Atomic Energy Levels (National Bureau of Standards, 1949), Vol. I.

M-3 B. L. Morgan and L. Mandel, Phys. Rev. Letters 16, 1012 (1966).

O-1 A. I. Odintsov, Opt. Spectry. (USSR) 14, 172 (1963).

O-2 Yu. I. Ostrovskii and N. P. Penkin, Opt. Spectry. (USSR) 10, 219 (1961).

R-1 N. F. Ramsey, Molecular Beams (Clarendon Press, Oxford, 1956), Chap. XIV.

R-2 J. F. Rendina, Rev. Sci. Instr. 34, 813 (1963).

R-3 O. W. Richardson, Molecular Hydrogen and Its Spectrum (Yale, 1934), Sec. 29.

R-4 B. L. Robinson and L. Madansky, Phys. Rev. 88, 1065 (1952).

S-1 E. Schatzman, Ann. Astrophys. (Paris) 28, 111 (1965).

S-2 P. A. Schilpp, ed., Albert Einstein: Philosopher-Scientist, Library of Living Philosophers, Vol. VII (Evanston, 1949), p. 235.

S-3 L. N. Shabanova, Opt. Spectry. (USSR) 15, 450 (1963).

S-4 W. W. Smith and A. Gallagher, Phys. Rev. 145, 26 (1966).

S-5 M. N. Smolkin and N. B. Berdnikov, Opt. Spectry. (USSR) 14, 220 (1963).

W-1 K. Watanabe and E. C. Y. Inn, J. Opt. Soc. Am. 43, 32 (1953).

W-2 J. A. Wheeler, Ann. N. Y. Acad. Sci. 48, 219 (1946).

W-3 A. Wightman, Phys. Rev. 74, 1813 (1948).

W-4 J. G. Winans and E. C. G. Stuekelberg, Proc. Natl. Acad. Sci. U. S. 4, 867 (1928).

W-5 C. S. Wu and I. Shaknov, Phys. Rev. 77, 136 (1950).

Y-1 C. N. Yang, Phys. Rev. 77, 242 (1950).